이학박사 학위논문

Control of Bio-Membrane Activity According to Light-Induced Structural Changes of Peptides

빛에 의한 펩타이드의 구조적 변화에 따른 생체막 활성 조절

2021 년 2 월

서울대학교 대학원

화학부 생화학 전공

김 규 찬

Control of Bio-Membrane Activity According to Light-Induced Structural Changes of Peptides

지도교수 이연

이 논문을 이학박사 학위논문으로 제출 함

2021 년 2 월

서울대학교 대학원

화학부 생화학 전공

김 규 찬

김규찬의 박사학위논문을 인준함

2021 년 2 월

위 원 장 이 현 우 (인)

부위원장 이 연 (인)

위 원 홍 종 인 (인)

위 원 유 재 훈 (인)

위 원 최 수 혁 (인)

Abstract

Control of Bio-Membrane Activity According to Light-Induced Structural Changes of Peptides

Kim, Gyu Chan

Department of Chemistry, Biochemistry

Graduate School of Natural Science

Seoul National University

Peptides, generally consisted of less than 50 amino acids linked by amide bonds, form secondary structure by the pattern of hydrogen bonds between the amino hydrogen and carboxyl oxygen atoms in the peptide backbone. Two most common secondary structures of peptide are alpha(α)-helix and beta(β)-sheet. In biological function, secondary structure of peptide arranged in tertiary structure of protein often bound to ligands such as coenzymes and cofactors, or to another macromolecule such as DNA or RNA to complex macromolecular assemblies. Therefore, change of secondary structure of peptide can be expected to have different biological functions.

Light is a physical stimulus that can regulate in an extraordinary spatiotemporal manner compared to chemical or biological stimuli. Especially, the light signal can be focused within sub-micrometer range spatial resolution and illuminated at a fixed wavelength and by a sub-femtosecond pulse. Therefore, using a light-responsive chemical bond can be cleaved or isomerized at a specific time and location to activation on demand is an attractive strategy for high selectivity.

In this thesis, two most common secondary structures of peptide; α-helix and β-sheet were controlled and studied to prove the relationship between the structural change and their bioactivity. 1) α-helix controlled by photo-isomerized azobenzene (Ab) incorporated to LK cell-penetrating peptides (CPPs) and 2) β-sheet changed by photo-cleavage of *ortho*-nitro benzyl (*o*-Nb)groups on Arenicin-1 (AR-1) antimicrobial peptides (AMPs). These two different structural and activity of peptide were controlled to change their secondary structures resulting in showing different biological activity.

Firstly, among various of peptides, the LK peptide, consisting of leucine (Leu, L) and lysine (Lys, K), is representative amphipathic and α-helical peptide. It has been reported that LK peptide having well-aligned cationic and hydrophobic faces show remarkable efficient cell-penetrating ability even at low nano-molar concentration. However, not only the effective cell penetration, but also specific discrimination of selective targeting is important because lack of selectivity can cause unexpected situations in vivo. Thus, for light-switchable activities of cell

penetrating peptides, azobenzene (Ab) moieties were incorporated to LK peptide. Ab shows a reversible configurational change between *trans*- and *cis*- of N=N bonds, depending on the wavelength used. Since the molecular dimension of the Ab moiety is significantly changed during the interconversion between *trans*- and *cis*-configurations, the LK peptide conformation with Ab linkers was dramatically changed upon the appropriate wavelength irradiation. As a result, The LK peptides linked with Ab-staple allow to complete reorganization of the helical structure, which results in change in cell penetrating ability. Thermally stable *trans* isomers of Ab stretches the LK peptide destabilizing helical structure and disrupts cell penetrating abilities, while corresponding *cis* isomers stabilizing helicity show stronger activities of cell penetration.

Secondly, Arenicin-1 (AR-1), is an antimicrobial peptide isolated from marine lugworm *Arenicola marina*, has a high positive charges with 6 arginine (Arg, R) residues with a single disulfide bond between Cys3 and Cys 20. AR-1 adopts the twisted β-hairpin structure playing important role in high antibacterial activity but it also displays hemolytic activity against human red blood cells. In order to develop more bacterial cell selective peptide, light-responsive chemical bonds can be cleaved by light irradiation were applied to AR-1. *O*-nitrobenzyl (*o*-Nb) group has been used as photo-protecting groups (PPGs), which can temporarily mask the original bioactivities of peptides. Two *o*-Nb groups were conjugated on thiol functional group of Cys3 and Cys20 on AR-1 respectively, interrupt forming disulfide bridge in consequence less

active against bacterial cells than original form of AR-1. Whereas, irradiation with the light of the appropriate wavelength removes the *o*-Nb groups and regenerates the native functional group in the peptide resulting in recovered the antimicrobial activity.

This behaviors of light-induced control of cell penetrating activities and antimicrobial activities by structural changes of peptides suggest that photo-responsive cell penetrating peptides and antimicrobial peptides may afford new opportunities to regulate delivery into cells and to develop new therapies for diseases killing bacteria cells with less side effects on surroundings.

Keyword: Alpha(*α*)-helix, Cell-Penetrating Peptides (CPPs), Azobenzene (Ab), Beta(*β*)-sheet, Antimicrobial Peptides (AMPs), *o*-Nitrobenzyl (*o*-Nb).

Student Number: 2015-30097

Contents

Abstract ii
Contents vi
List of Figures ix

PART 1. Photo-Switching of Cell Penetration of Amphipathic Peptides by Control of Alpha-Helical Conformation

1. Abstract 1
2. Introduction 3
3. Experimental Section 7
3.1 Materials 7
3.2 Synthesis of Azobenzne linker 8
3.3 ^{1}H NMR Spectra of Azobenzene linker 9
3.4 Synthesis of LK Peptides 11
3.5 Stapling of LK Peptides with Azobenzene linker 17
3.6 Photo-induced UV/Vis Spectral change 20
3.7 Photo-induced Circular Dichroism (CD) change 22
3.8 FACS Analysis for peptide penetration 24
3.9 Confocal Laser Scanning Microscopy (CLSM) 26
3.10 Dynamic Light Scattering (DLS) 28
3.11 Cytotoxicity assay 30
4. Results and Discussion 32
4.1 Preparation of the Ab-stapled LK peptide 32
4.2 Photo-induced conformational change of the Ab-LK peptide 35

4.3 Photo-switching of cell penetrating activity of the Ab-LK peptide. 38
4.4 Photo-switching of association behaviors of the Ab-LK peptide 42
4.5 Cytotoxicity and stability of the Ab-LK peptide. 45
5. Conclusion 47
6. Reference 48

PART 2. Photo-Control of Beta-Sheet with Antimicrobial Activity of Arenicin-1

1. Abstract 54
2. Introduction 56
3. Experimental Section 59
3.1 Materials 59
3.2 Synthesis of Azobenzne linker 60
3.3 ^{1}H NMR Spectra of Azobenzene linker 61
3.4 Stapling of AR-1 with Azobenzene linker 63
3.5 Photo-induced UV/Vis spectral change 65
3.6 Photo-induced Circular dichroism (CD) 67
3.7 Minimum inhibitory concentration (MIC) test 69
4. Results and Discussion 71
4.1 Preparation of the Ab-stapled AR-1 peptide 71
4.2 Photo-induced conformational change of the Ab-AR-1 peptide 73

4.3 Photo-switching of antimicrobial activity of the Ab-AR-1 peptide. 75
4.4 Preparation of the Photo-caged *o*-Nb-AR-1 peptide. 77
4.5 Photo-induced conformational change of the *o*-Nb-AR-1 peptide 78
4.6 Photo-cleavage change of the o-Nb-AR-1 peptide. 80
4.7 Photo-induced antimicrobial activity change of the *o*-Nb-AR-1 peptide. 82
5. Conclusion 84
6. Reference 85

List of Publication 89
Abstract (국문초록) 90

List of Figures.

PART 1. Photo-Switching of Cell Penetration of Amphipathic Peptides by Control of Alpha-Helical Conformation

Scheme 1. Synthetic scheme of Ab-diacetyl chloride.....8
Figure 1. ^{1}H NMR spectra (500MHz, 4 mM in DMSO-d_6, 25℃) of Ab-diacetyl chloride. 10
Figure 2. The HPLC chromatogram of Ac-LK(7,11) (top), and mass spectrum. (bottom) 14
Figure 3. The HPLC chromatogram of TAMRA-LK(7,11) (top), and mass spectrum. (bottom) 15
Figure 4. The HPLC chromatogram of TAMRA-Tat (top), and mass spectrum.(bottom) 16
Scheme 2. Synthetic scheme of Ab-LK peptide.....17
Figure 5. The HPLC chromatogram of Ac-Ab-LK(7,11) (top), and mass spectrum. (bottom) 18
Figure 6. The HPLC chromatogram of TAMRA-Ab-LK(7,11) (top), and mass spectrum. (bottom).....19
Figure 7. UV/Vis absorption spectral changes of acetylated Ab-LK (7,11) (25 μM in 50 mM PBS pH 7.4, 25℃) upon irradiation at 365 nm and 440 nm, respectively 21
Figure 8. CD spectral changes of acetylated Ab-LK(7,11) (100 μM in 50 mM PBS and 50% TFE) upon irradiation 365 nm and 440 nm, respectively.. 23
Figure 9. FACS results for 100 nM of Tamra Ab-LK (7,11) in HeLa cells. Each histogram plots a TAMRA fluorescence intensity

(horizontal axis) against the number of events detected (vertical axis) and represents (a) control, (b) in the dark *trans*-Ab-LK, (c) UV-irradiated *cis*-Ab-LK, and (d) integrated form.....25
Figure 10. CLSM images of HeLa cells after 4 h treatment of each Tamra-labeled Ab-LK at 200 nM. Nucleus was stained with Hoechst 3342 (blue).....27
Figure 11. DLS data of Acetylated Ab-LK(7,11) (1 μM in PBS solution). Peak shift from *trans* isomer (red) to a larger particle diameter with UV irradiated *cis* isomer (blue). Vis irradiation returning into *trans* isomer decreases the particle size (green) and re-irradiation UV (orange) and Vis (purple) were performed as repeated cycles. 29
Figure 12. Relative viability of HeLa cells after 2 h treatment with each TAMRA-labeled Ab-LK at 10, 100 and 1000 nM. Each error bar represents the standard deviation (n = 3). UV-irradiated Ab-LK peptide (blue), in the dark Ab-LK peptide (red), and non Ab-stapled LK peptide (green) show not very toxicity on HeLa cells at these concentrations.. 31
Figure 13. The wheel diagram of the Ab-stapled LK peptide (Ab-LK) and the conceptual scheme for photo-switching of the α-helical structure.. 34
Figure 14. Reversible photo-switching of the Ab-LK peptide. Solid red and dashed blue lines indicated the data from UV- and Vis-irradiated Ab-LK peptides, respectively. (a) UV/Vis spectra, (b) Circular Dichroism (CD) spectra of the Ab-LK peptide. (c) α-Helical change (black solid) and cis ratios (blue dash) of Ab-LK peptide by serial UV-Vis irradiation. (d) Summary of *cis* ratios and α-helicities of the Ab-LK peptide upon UV-Vis

irradiation. The CD spectra were measured in phosphate buffer solution (50 mM, PBS pH 7.4) with 50% 2,2,2-trifluoroethanol (TFE) at room temperature... 37
Figure 15. Photo-switching of cell penetration of the Ab-LK peptide on HeLa cells. (a) Percentage of fluorescence-positive cells after 2 h incubation with various TAMRA-labeled cell-penetrating peptides at 100 nM. (b) Mean fluorescence intensity (MFI) of HeLa cells treated with various TAMRA-labeled cell-penetrating peptides for 2h. Each error bar represents the standard deviation (n = 3). The markers (*) and (**) indicate $p < 0.05$ and $p < 0.01$, respectively. (c) CLSM images of HeLa cells treated with TAMRA-labeled (red) *trans* Ab-LK, *cis* Ab-LK,,and trans-Ab-LK in situ irradiated by UV for 5 min. The nucleus was stained with Hoechst 33442 (blue). White arrows indicate TAMRA fluorescence signals (red) in the figure. 39
Figure 16. FACS results for 100 nM of Tamra Ab-LK (7,11) in various cell lines; HeLa, CHO-K1, HEK 293T, and MDA-MB-231. Tamra LK (white), non-irradiated Tamra Ab-LK (7,11) (red), and UVirradiated Tamra Ab-LK (7,11) (blue) were treated on the cell lines for 2 hours. (a) Percentage of fluorescence-positive cells and (b) mean fluorescence intensity (MFI) of peptide-treated cells. Each error bar represents the standard deviation (n = 3). The markers (*), (**) and (***) indicate $p < 0.05$, $p < 0.01$, and $p < 0.001$, respectively.....41
Figure 17. Photo-switching of association-dissociation of the Ab-LK peptide and entry to cells. (a) Dynamic laser light scattering (DLS) size distributions of *trans* Ab-LK (red and green) and *cis* Ab-LK (blue and orange) (b) A proposed

mechanism of photo-switched cell penetration of the Ab-LK peptide. 44
Figure 18. Stability of non-stapled LK and Ab-LK after treatment with trypsin (1 wt %). Nonstapled LK and Ab-LK (1 mg/mL) were treated by 1 wt % of trypsin in a 50 mM Tris-HCl buffer (pH 8.0). After incubation at 37°C, the samples were analyzed by MALDI-TOF. (a) Non-stapled LK peptide and (b) stapled Ab-LK peptide 46

PART 2. Photo-Control of Secondary Structure with Antimicrobial Activity of Arenicin-1

Scheme 2. Synthetic scheme of Ab-diacetyl chloride 60
Figure 19. ^{1}H NMR spectra (500MHz, 4 mM in DMSO-d_6, 25℃) of Ab-diacetyl chloride 62
Figure 20. Mass spectrum of AR-1 (sequence: RWCVYAYRRVRGVLVRYRRCW) was obtained as white powder. MS ($M+H^+$) 2759.5 (calcd.), 2761.6 (found).....63
Figure 21. Mass spectrum of Ab-AR (sequence: Ab-RWCVYAYRRVRGVLVRYRRCW) was obtained as yellowish powder. MS ($M+H^+$) 3051.6 (calcd.), 3050.9 (found).....64
Figure 22. UV/Vis absorption spectral changes of Ab-AR-1 (25 μM in 50 mM PBS pH 7.4, 25℃) upon irradiation at 365 nm for 1, 3 min and 440 nm for 10 min, respectively.....66
Figure 23. CD spectral changes of AR-1 and Ab-AR-1 (100 μM in 50 mM PBS and 50% TFE) upon irradiation 365 nm for 5 min and 50℃ for 30 min, respectively.....68
Figure 24. Bacterial growth spectrum depending on concentration of AR-1 and Ab-AR-1 (0.5 to 32 μM incubated for 20h at 37℃)were measured the absorbance at 600 nm.....70
Scheme 3. General scheme of Ab-AR-1 peptide 72
Scheme 4. General scheme of Ab-AR-1 peptide 76
Figure 25. Sequence: *o*-Nb-RWCVYAYVRVRGVLVRYRRCW was obtained at 22.4 min as white powder with eluted 20 to 50% of ACN 0.1% TFA for 30 min. The HPLC chromatogram of *o*-Nb-AR-1 is shown (left, bottom) with detection at 220 nm (black)

and 280 nm (red). MS ($M+Na^+$) 3036.5 (calcd.), 3038.9 (found) (bottom) 77
Figure 26. (a) UV/Vis absorption spectral changes of *o*-Nb-AR-1 (25 μM in 50 mM PBS pH 7.4, 25℃) upon irradiation at 280 nm for 5 min. (b) CD spectral changes of Ab-AR-1 (100 μM in 50 mM PBS and 50% TFE) upon irradiation 280 nm for 20 min..79
Figure 27. General scheme for photo-cleavage of *o*-Nb-AR-1 peptide and mass spectral changes of *o*-Nb-AR-1 upon irradiation at 280 nm for 1 min. MS ($M+H^+$) 3029.5 (calcd.), 3032.9 (found) (left, bottom). Irradiated *o*-Nb-AR-1 were found as photo-cleaved AR-1 ($M+H^+$) 2759.5 (calcd.), 2761.7 (found) (left, bottom) 81
Figure 28. Bacterial growth spectrum depending on concentration of AR-1 (black) and *o*-Nb-AR-1 (0.5 to 32 μM incubated for 20h at 37℃)were measured the absorbance at 600 nm. Non-irradiated *o*-Nb-AR-1 (red) and irradiated *o*-Nb-AR-1 (blue) were shown. 83

PART 1. Photo-Switching of Cell Penetration of Amphipathic Peptides by Control of Alpha-Helical Conformation

1. Abstract.

In this study, the light-induced control of cell penetrating activities of an amphipathic peptide, LK peptide mainly consisting of leucine (L) and lysine (K), by azobenzene (Ab)-mediated regulation of the secondary structure were reported. The *i*, and *i*+4 positions of the LK peptide was stapled with an Ab linker, and the geometrical conversion of the Ab-linker by UV-Vis irradiation induced a remarkable change of the alpha-helical conformation of the Ab-stapled LK peptide (Ab-LK). Moreover, their cell-penetrating activities were significantly dependent upon the irradiation wavelengths, resulting that UV-induced *cis* Ab-LK with a stabilized alpha-helical structure showed much higher cell-penetrating activity than Vis-induced *trans* Ab-LK with a destabilized structure at nano-molar concentrations, where the conventional CPPs such as Tat or oligoarginine cannot penetrate

cells with efficiency. Interestingly, the Ab-LK also showed dynamic association-dissociation behaviors depending upon the photo-irradiation; large multimeric structures were rapidly formed by UV irradiation but reversibly dissociated by Vis irradiation. It is supposed that the Ab-LK peptide can expose well-defined hydrophobic and cationic faces by UV-induced *cis*-Ab stapling to induce the formation of the associated structure and to enhance endocytic internalization effectively on the cell membrane, but too-long *trans*-Ab stapling might break the defined faces to induce the dissociation of the multimeric structure and lose the effective endocytosis-inducing ability.

2. Introduction

Peptide-based pharmaceuticals receive increasing attention from biomedical researchers because they have high potential to control biomolecular interactions with large and wide contacting areas. [1] Peptides can be easily synthesized by solid-phase peptide synthesis (SPPS) methods, and the 3D-structure can be readily predicted from the database of related protein structures.[2] Despite these advantages of peptide-based pharmaceuticals, their poor permeability through cell membranes and the instability in physiological fluids greatly hamper their accessibility to intracellular targets, thereby limiting their practical application.[3] Therefore, the targets of most peptide-based pharmaceuticals are confined to extracellular molecules with a short duration of action.[4] Various delivery and modification methods have been developed to overcome the intrinsic weak-points of peptides. Liposomes or nanoparticles have been used for encapsulation and intracellular delivery of peptides and proteins with limited success.[5] Chemical modifications such as introduction of hydrophobic moieties or protection from the action of peptidase might be other options for enhancing membrane permeability and stability.[6] The conformation

of peptide-based pharmaceuticals can be optimized for increasing permeability.[7]

Cell-penetrating peptides (CPPs) are popular because of their extraordinarily high cell permeability across the cell membrane.[8] Understanding the structural basis of cell-penetrating activity of CPPs may be helpful for the developing more permeable peptide-based pharmaceuticals or drug delivery vehicles. Thousands of CPP sequences have been reported; they are classified into two categories: multi-positively charged sequences with many lysine (K) and arginine (R) residues, *e.g.*, Tat or oligo-arginine, and amphipathic cationic sequences with both hydrophobic and positively charged residues, *e.g.*, penetratin or transportan.[9] Many amphiphatic CPPs have α-helical conformations with well-defined cationic and hydrophobic faces.[10]

Stapling techniques have been introduced for increasing structural stability of peptides.[11] Stapled peptides showed significant increase in binding affinity on the targets compared with the non-stapled ones and they also show an increase of resistance against enzymatic degradation mainly because of the structurally frozen conformation.[12] Stapled α-helical peptides showed much higher cell-penetrating activity than the non-stapled peptides.[13]

Improved α-helical property through stapling was considered to be the key factor for the enhanced cell penetration. Inspired from the structural characteristics of CPPs and stapled peptides with enhanced cell permeation, we expected that the cell-penetrating activity of peptides can be controlled by stimulus-dependent regulation of the α-helical conformation. As most CPPs and stapled peptides showed unbiased cell permeation irrespective of cell or tissue types,[14] stimulus-dependent control of the penetrating activity would be a significant progress for obtaining highly specific peptide-based pharmaceuticals or CPP-based drug delivery carriers for practical applications.

The light was selected as a triggering signal for controlling the α-helical conformation of peptides. Because light is a spatiotemporally focusable stimulus, we believed that it might be an appropriate signal for sensitive control of the peptide secondary structure as well as penetration activity in the bio-system. Azobenzene (Ab) is a well-known photo-responsive moiety showing reversible *cis-trans* structural conversion responding to UV and Vis light.[15] The difference of the distance between the para-substituents in the Ab moieties (≈ 10Å) during the geometric conversion is sufficient for inducing large structural changes in

peptides.[16] α-helical conformations could be reversibly formed and deformed by photo-switching of Ab moieties that were conjugated to carefully selected amino acid residues.[17]

In a previous study, it is observed that an α-helical amphipathic peptide mainly consisting of leucine (L) and lysine (K) as the hydrophobic and cationic faces, respectively, namely the LK peptide, exhibited much higher cell-penetrating activity than Tat or oligo-arginine at sub-micromolar concentrations.[18] Herein, photo-switchable cell-penetrating activity of LK peptides based on Ab-mediated changes of alpha-helical conformation is described (**Figure 17**). Light irradiation at appropriate wavelengths led to critical but reversible reorganization of the helical structure through *cis-trans* isomerization, which resulted in notable switching of the cell-penetrating activity.

3. Experimental Section

3.1 Materials

All chemicals were purchased from commercial suppliers and used without further purification. 4, 4’ −Diaminoazobenzene was purchased form Alfa Asear (US) and chloroacetyl chloride was purchased from TCI (Japan). Triethylamine (TEA) was purchased form Aldrich (US) and sodium sulfate (Na_2SO_4) was purchased form Daejung (South Korea). Chloroform (CH_3Cl), dimethylforamide (DMF), dichloromethane (DCM) and hexane were purchased from Samchun Chemical (South Korea). *N*− α −Fmoc protected L−amino acids, Rink Amide MBHA resin (0.064 mmol/g loading), and benzotriazole−1−yl−oxy−tris−pyrrolidino−phosphonium hexafluorophosphate (PYBOP) were purchased from Novabiochem (San Diego, CA, USA). *N*,*N*−dimethylformamide (DMF), dichloromethane (DCM), *N*,*N*−diisopropylethylamine (DIPEA), trifluoroacetic acid (TFA), triisopropylsilane (TIS), and piperidine were purchased from Sigma−Aldrich (St. Louis, MO, USA). *N*,*N*’ −1,4−phenylenedimaleimide and 1,2−ethanedithiol (EDT) were purchased from TCI (Japan). *n*−Hexane and diethyl ether were purchased from DAEJUNG (Siheung, Gyeonggi, Korea).

3.2 Synthesis of Azobenzne linker

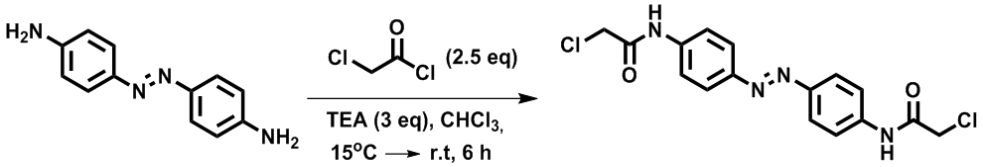

Scheme 1. Synthetic scheme of Ab−diacetyl chloride.

4,4’−Diaminoazobenzene (200 mg, 0.94 mmol) was dissolved in $CHCl_3$ (100 mL), then cooled to 15° C. Triethylamine (394 μL, 3 eq) was added and chloroacetyl chloride (187 μL, 2.5 eq) was added to the mixture. The mixture was stirred at room temperature for 6 h. The reaction was quenched by addition of water (100 mL). The organic layer was separated, washed with water twice (2 × 100 mL), dried over sodium sulfate (Na_2SO_4). The solvent was evaporated in vacuum to afford brown solid. The crude product was recrystallized in DMF/DCM/hexane (1:20:20) to yield yellow solid. 93% (320 mg). ^{1}H−NMR (500 MHz, DMSO−d_6, 298K, ppm) δ 10.64 (s, NH), 7.88 (d, J = 10.0 Hz, 2H), 7.81 (d, J = 10.0 Hz, 2H), 4.31 (s, 2H). ^{13}C−NMR (500 MHz, DMSO−d_6, 298K, ppm) 164.97, 148.01, 141.09, 123.40, 119.62, 43.54.

3.3 ^{1}H NMR spectra of Azobenzene linker

Stock solution (4 mM in DMSO-d_6) of Ab-diacetyl chloride was prepared in a vial in the dark. An aliquot (400 μL) of the solution was transferred to a NMR tube and ^{1}H NMR spectrum was recorded for the *trans* isomer. After the measurement, the solution was transferred to a quartz cell and irradiated UV light for 5 min, which resulted in *trans* to *cis* isomerization. Irradiation was carried out using a 100W high-pressure mercury lamp (Lichtzen, South Korea) equipped with fiber optics and band-pass filters (Edmund optics, US). For UV irradiation, a 357 nm band-pass filter with a 48 nm full width-half-max (FWHM) was used (OD > 6.0). ^{1}H NMR spectrum was recorded and the population of the cis isomer at the photo-stationary state (PSS' s) was determined by the ^{1}H NMR integration of each shifted signals.

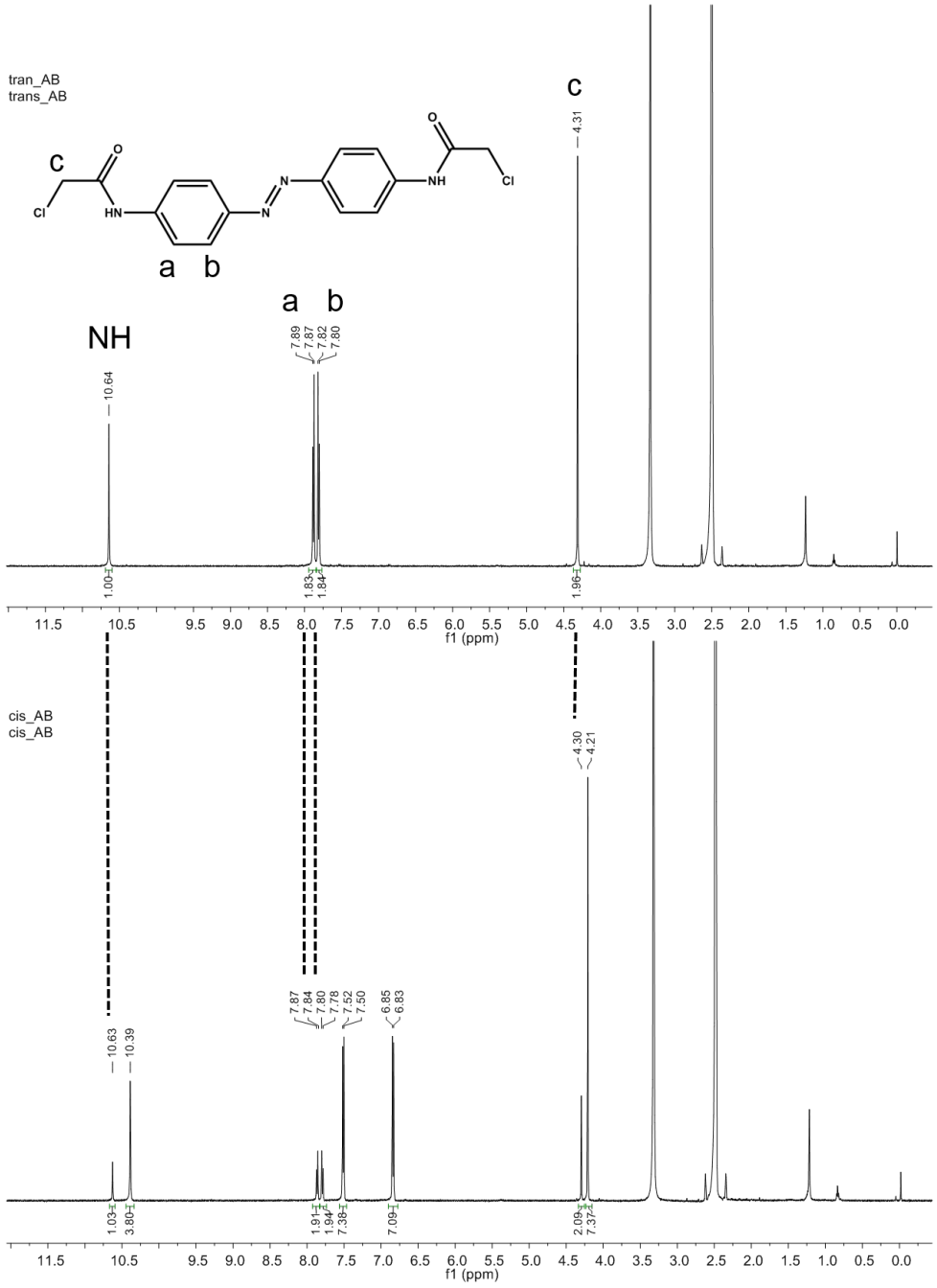

Figure 1. ^{1}H NMR spectra (500MHz, 4 mM in DMSO-d_6, 25℃) of Ab-diacetyl chloride. *Trans* isomer (top) and *cis* isomer (bottom); *trans* : *cis* = 21 : 79 at PSS.

3.4 Synthesis of LK Peptides

LK (7, 11) peptide (sequence: LKKLLKCLKKCLKLAG) was synthesized by using an Fmoc-based solid-phase peptide synthesis protocol with Rink Amide MBHA resins. Peptides were synthesized in the scale of 64 mol. Rink Amide MBHA resins (100 mg, 0.059 mmol, 0.064 mmol/g loading) were deprotected with 20% piperidine in DMF (2 mL) and washed with DMF and DCM solvents (3 × 2 mL). Then, Fmoc protected first amino acid, glycine (105.2 mg, 0.354 mmol), PYBOP (184.2 mg, 0.354 mmol), and DIPEA (62 L, 0.354 mmol) were added to the resin suspension in DMF (2 mL) and stirred at room temperature for 3 h. The byproducts of reaction were removed by washing with DMF and DCM solvents (3 × 2 mL). The completeness of the reaction was checked by using the 2,4,6-trinitrobenzenesulfonic acid (TNBS) test after the coupling. After the first coupling, Fmoc-protected first amino acid was deprotected with 20% piperidine in DMF, and the byproducts of reaction were removed with DMF and DCM solvents (3 × 2 mL). The coupling and deprotection steps were repeated with different Fmoc-protected amino acids sequentially until deprotection of the last Fmoc-protected amino acids. The deprotected resin-bound peptide was washed with DMF and DCM solvents. The N-terminus

of the peptide was then acetylated or conjugated with a fluorescent dye. For acetylation, the peptide was reacted with acetic anhydride (0.3 mmol, 29 L), N-hydroxybenzotriazole (HOBT) (0.3 mmol, 41 mg) and DIPEA (0.3 mmol, 52L) in a solvent (DMF:DCM) (2 mL, v/v= 90:10). The reaction mixtures were stirred for 2 h at room temperature. For the dye-conjugation, the peptide was reacted with 5-carboxytetramethylrhodamine (TAMRA) (0.3 mmol, 129 mg), HOBT (0.3 mmol, 41 mg) and DIPEA (0.3 mmol, 52L) in a solvent (DMF:DCM) (2 mL, v/v= 90:10). The reaction mixtures were stirred for 2 h at room temperature. Peptides were cleaved from the solid support by treatment with a mixture consisting of TFA/TIS/EDT/water (2 mL, v/v= 94:1:2.5:2.5) for 2 h at room temperature. The cleaved resin was then separated by filtration and further washed with TFA (1 mL). The filtrate solution was concentrated by a nitrogen gas and precipitated into n-hexane and diethyl ether mixture at the equal volume (v/v = 50:50). The resulting suspension was centrifuged at 1,500 rpm for 15 min at 4℃. After the supernatant was carefully decanted, the pellet was dissolved in DMF (1 mg/mL). Finally, the peptides were purified with HPLC (Agilent 1100 series) with a Zorbax C18 (3.5 m, 4.6 x 150 mm) column. For the mobile phase, Solution A (water with

0.1% v/v TFA) and Solution B (acetonitrile with 0.1% v/v TFA) were used as eluent solutions. LK (7, 11) peptide was eluted at 40–60% of Solution B. The peptide was lyophilized affording white or pink powder (4~5 mg, 40% yield). Mass Spectra of peptides were obtained using a Voyager TM MALDI-TOF mass instrument (Applied Biosystems). The HPLC chromatogram of each LK (7, 11) peptides were shown. (>98% purity).

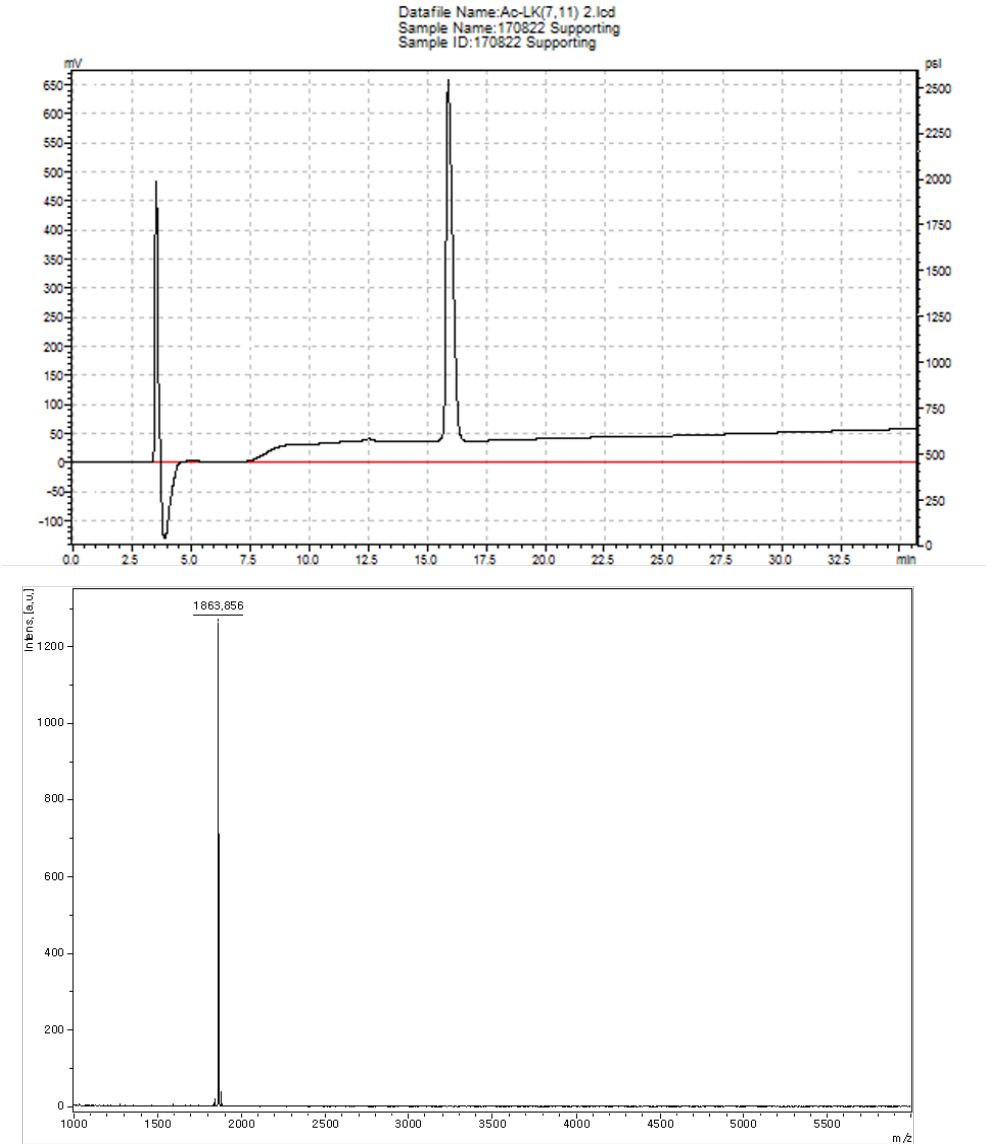

Figure 2. Acetylated LK(7,11) (sequence: Acetyl-LKKLLKCLKKCLKLAG) was obtained at 15.9 min as white powder with eluted 40 to 60% of ACN 0.1% TFA solution for 30 min. The HPLC chromatogram of Ac-LK(7,11) is shown (top) with detection at 220 nm (black) and 365 nm (red). MS ($M+Na^+$) 1864.2(calcd.), 1863.8 (found). (bottom)

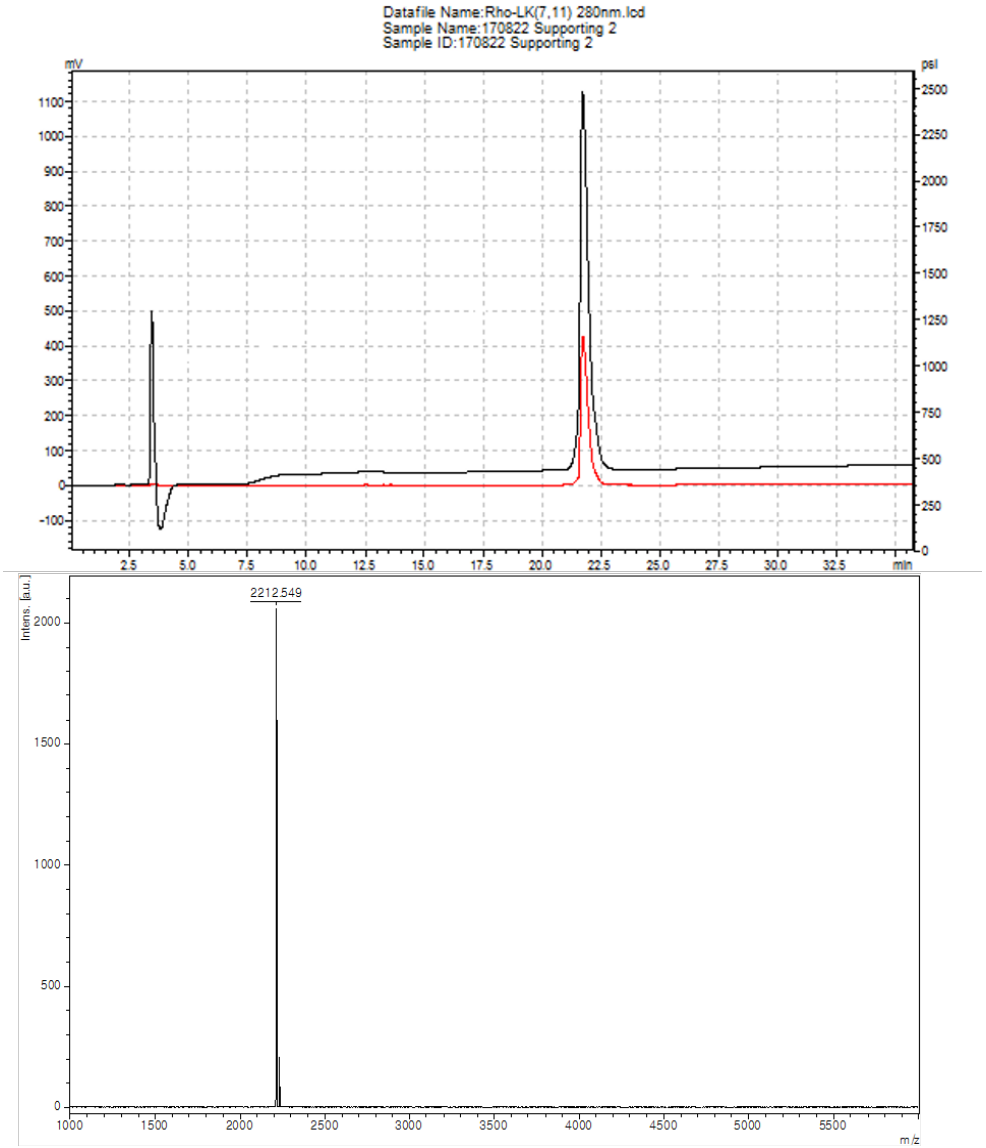

Figure 3. TAMRA-labeled LK(7,11) (sequence: TAMRA-LKKLLKCLKKCLKLAG) was obtained at 21.7 min as pink powder with eluted 40 to 60% of ACN 0.1% TFA solution for 30 min. The HPLC chromatogram of TAMRA-LK(7,11) is shown (top) with detection at 220 nm (black) and 365 nm (red). MS ($M+H^+$) 2214.3 (calcd.), 2212.5 (found). (bottom)

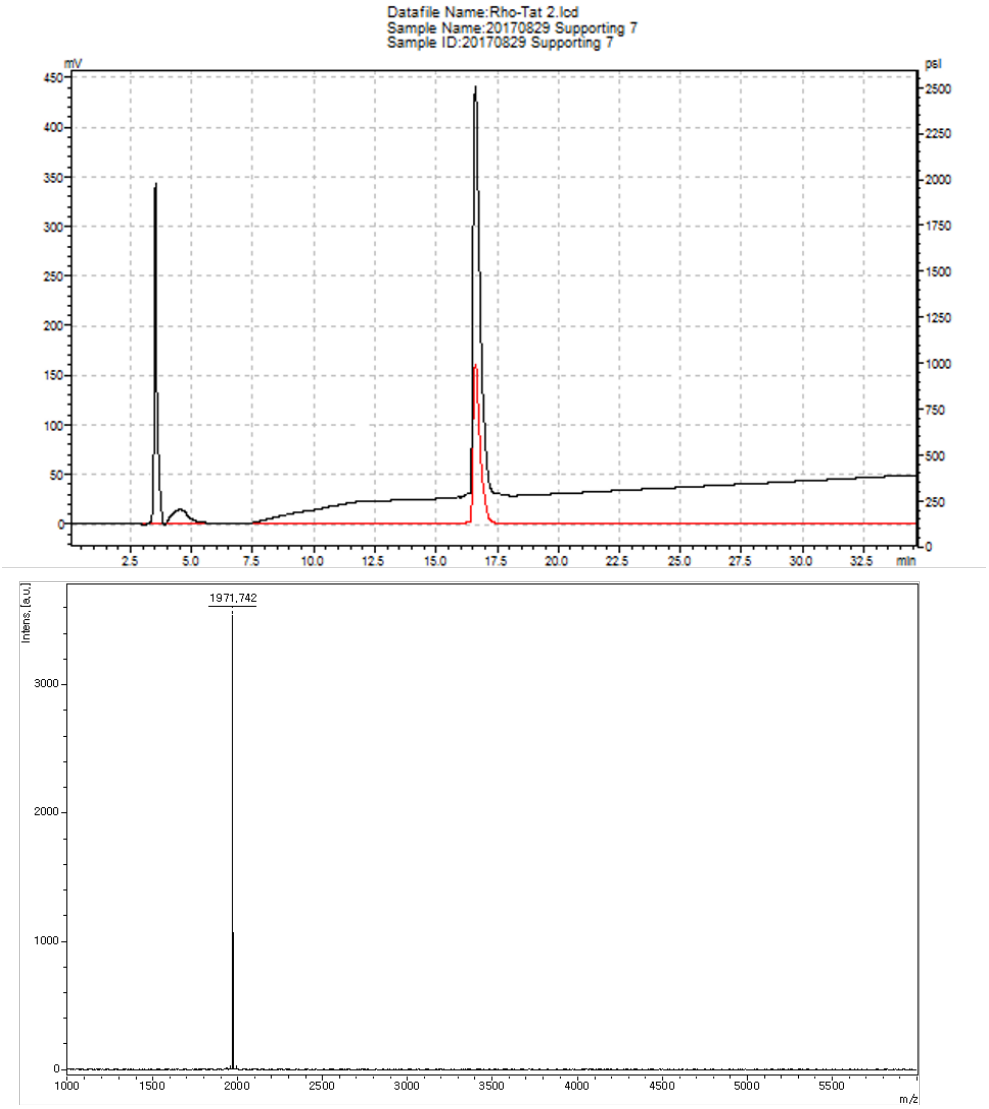

Figure 4. TAMRA-labeled Tat (sequence: TAMRA-YGRKKRRQRRR) was obtained at 16.6 min as pink powder with eluted 20 to 40% of ACN 0.1% TFA for 30 min. The HPLC chromatogram of TAMRA-Tat is shown (top) with detection at 220 nm (black) and 280 nm (red). MS ($M+H^+$) 1973.1 (calcd.), 1971.7 (found) (bottom)

3.5 Stapling of LK Peptides with Azobenzene linker

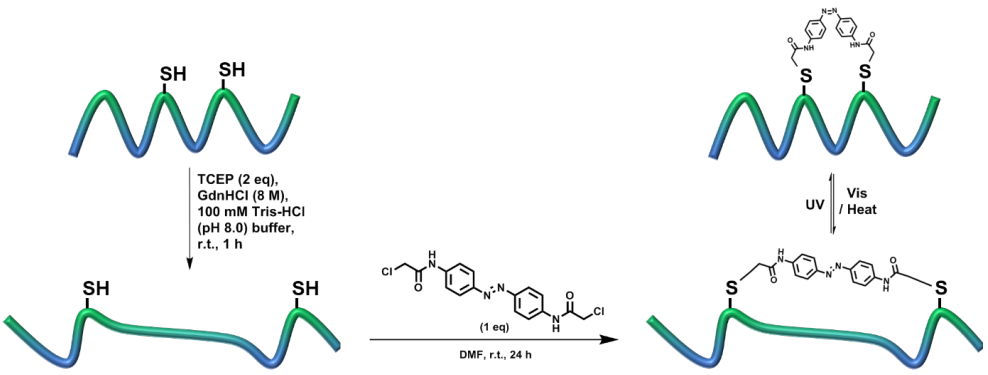

Scheme 2. Synthetic scheme of Ab-LK peptide.

Intramolecular stapling of the acetylated or TAMRA-labeled LK (7, 11) peptide (sequence: LKKLLKCLKKCLKLAG) was performed in the presence of guanidine hydrochloride (GdnHCl) to disrupt the α-helical conformation during the coupling reaction. The LK (7, 11) peptide (0.5 mM) and tris(2-carboxyethyl)phosphine hydrochloride (TCEP) (1 mM) were dissolved in an aqueous solution containing 100 mM Tris-HCl and 8 M GdnHCl at pH 8.0. The reaction mixture was allowed to be stirred for an hour at ambient temperature. The synthesized Ab-diacetyl chloride (0.5 mM) was dissolved in DMF and the solution was mixed with the peptide solution. After 24 h-stirring, the stapled peptide (Ab-LK) was purified using HPLC with the same protocol described above.

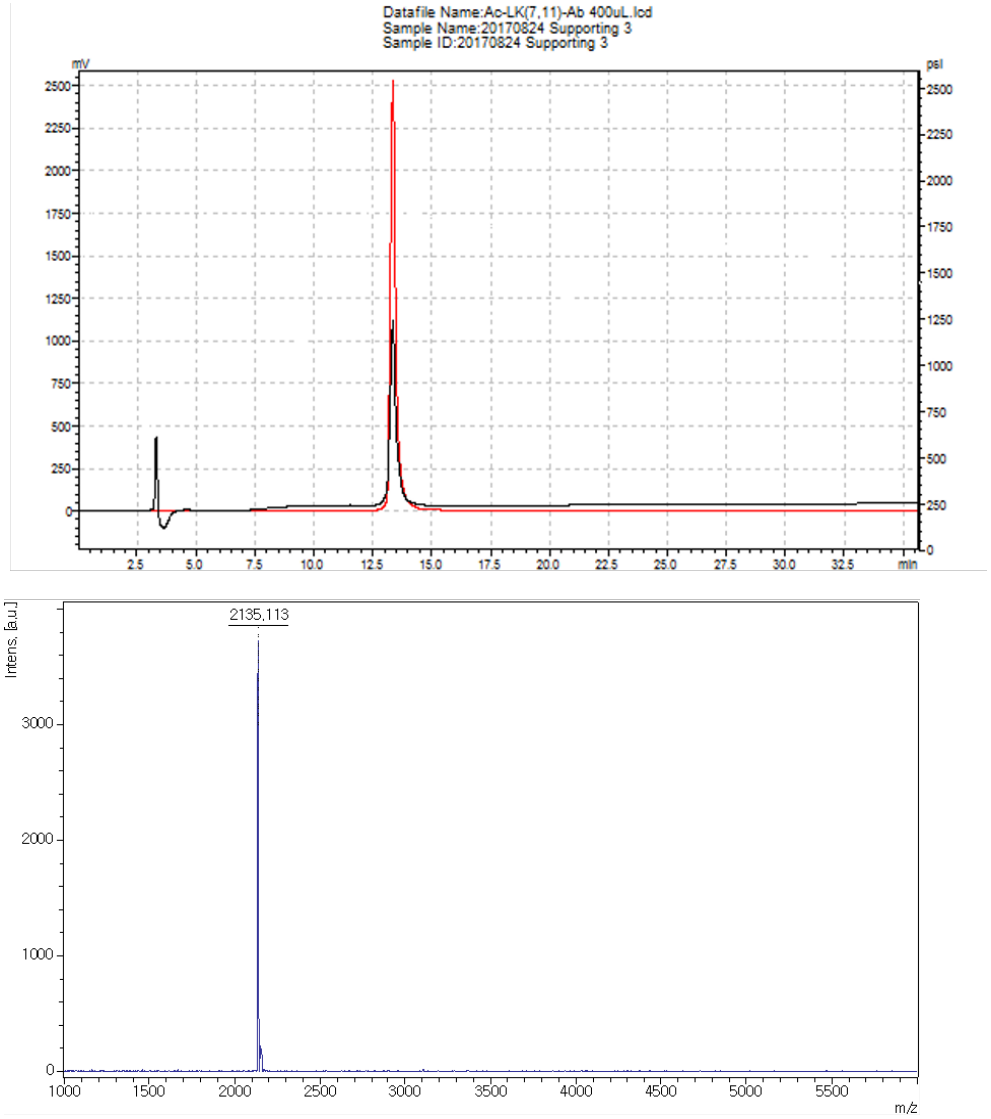

Figure 5. Acetylated Ab-LK(7,11) (sequence: Acetyl-Ab-LKKLLKCLKKCLKLAG) was obtained at 13.4 min as yellow powder with eluted 40 to 60% of ACN 0.1% TFA solution for 30 min. The HPLC chromatogram of Ac-Ab-LK(7,11) is shown (top) with detection at 220 nm (black) and 365 nm (red). MS ($M+H^+$) 2143.3 (calcd.), 2135.1 (found). (bottom)

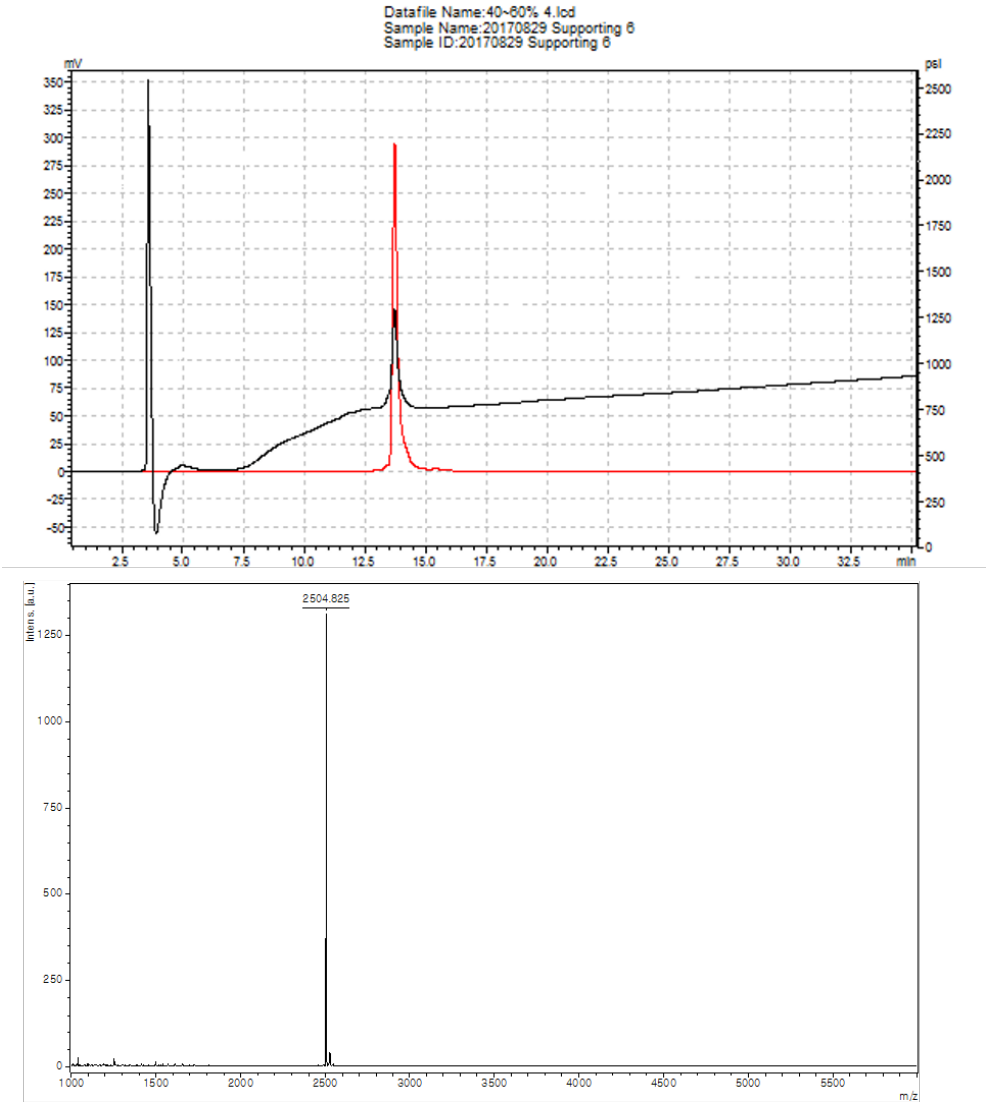

Figure 6. TAMRA-labeled Ab-LK(7,11) (sequence: TAMRA-Ab-LKKLLKCLKKCLKLAG) was obtained at 13.7 min as pink powder with eluted 40 to 60% of ACN 0.1% TFA for 30 min. The HPLC chromatogram of TAMRA-Ab-LK(7,11) is shown (top) with detection at 220 nm (black) and 365 nm (red). MS ($M+H^+$) 2506.4 (calcd.), 2504.8 (found) (bottom)

3.6 Photo-induced UV/Vis spectral change

Measurements of UV/Vis absorption spectra were performed in a high precision quartz cell (Hellma Analytics) using a UV/Vis spectrophotometer (JASCO, V-650). Absorption was measured from 200 to 600 nm. Stock solution (25 μM in a 50 mM phosphate buffer solution (PBS) pH 7.4) of acetylated Ab-LK (7,11) peptide was prepared in a vial in the dark. An aliquot (300 μL) of the solution was transferred to a UV quartz cell and UV/Vis absorption spectrum was recorded for the trans isomer. After measurement, the solution was irradiated UV light for 5 min, which resulted in trans to cis isomerization. Irradiation was carried out using a 100 W high-pressure mercury lamp (Lichtzen, South Korea) equipped with fiber optics and a 357 nm band-pass filter (Edmund optics, US). UV/Vis spectrum was recorded for the cis isomer and then solution was re-irradiated by the lamp with a 440 nm band-pass filter for 10 min for the recovery to trans conformation. These irradiation UV/Vis cycles were repeated twice and the population of the cis isomer at the photo-stationary state (PSS' s) was determined by the intensities of λmax (365 nm) signals assuming that trans isomer exists as 100 % and the

maximum changes would be the difference between absorbance values at 365 nm for trans isomer and the background.

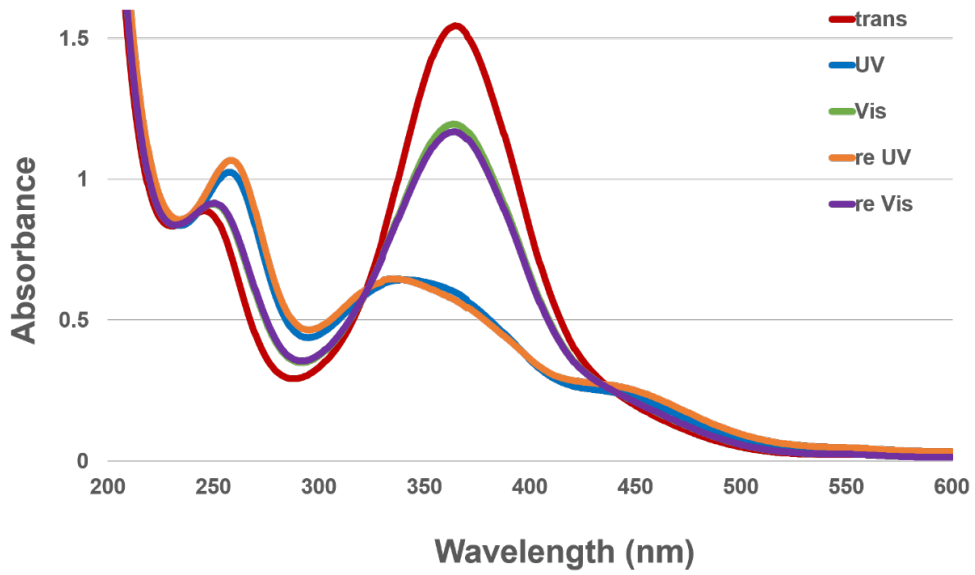

$$trans\ ratio\ (\%) = \frac{(Abs_{measure} - Abs_{No\ Azo})}{(Abs_{trans} - Abs_{No\ Azo})} \times 100\ (\%)$$

	$Abs_{365\ nm}$	*trans* : *cis*
Ac-LK(7,11) (No Azo)	0.270065	–
Ac-LK(7,11)-Ab trans	1.54441	100 : 0
Ac-LK(7,11)-Ab UV	0.598346	26 : 74
Ac-LK(7,11)-Ab Vis	1.19495	72 : 28
Ac-LK(7,11)-Ab re UV	0.51639	19 : 81
Ac-LK(7,11)-Ab re Vis	1.16803	70 : 30

Figure 7. UV/Vis absorption spectral changes of acetylated Ab-LK (7,11) (25 μM in 50 mM PBS pH 7.4, 25℃) upon irradiation at 365 nm and 440 nm, respectively.

3.7 Photo-induced circular dichroism change

Measurements of CD spectra were performed using a Circular Dichroism spectropolarimeter (JASCO, J-815) with a 1.0 mm path-length cell (JASCO). CD was scanned from 190 to 260 nm with a set-up of 0.2 s-integration, 1 nm-step resolution and 1 nm-bandwidth. The results from three scans were averaged. α-helicity of acetylated Ab-LK (7,11) peptide was measured in phosphate buffer solution (50 mM PBS pH 7.4) with 50% 2,2,2-trifluoroethanol (TFE) as a membrane-mimic condition at room temperature. A stock solution (50 μM in PBS and 50% TFE) of acetylated Ab-LK (7,11) peptide was prepared in a vial in the dark. An aliquot (300 μL) of the solution was transferred to a cell and the CD spectrum was recorded for the trans isomer. After measurement, the solution was irradiated by UV light for 5 min, which resulted in trans to cis isomerization. Irradiation was carried out using a 100W high-pressure mercury lamp (Lichtzen, South Korea) equipped with fiber optics and a 357 nm band-pass filter (Edmund optics, US). After record for the cis isomer and the solution was re-irradiated by the lamp equipped with a 440 nm band-pass filter for 10 min for cis to trans isomerization. These

irradiation cycles were repeated twice and the change of α-helicity was calculated.

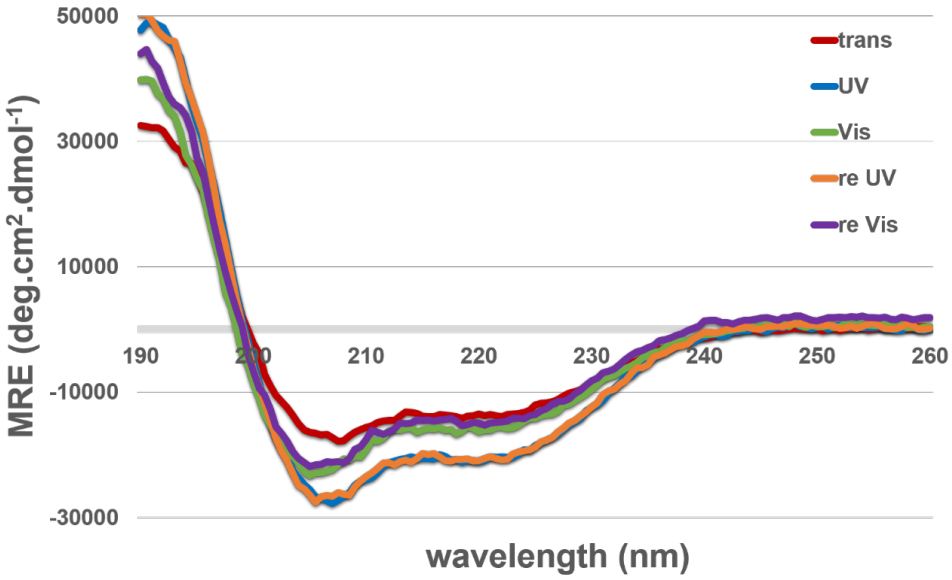

$$MRE\ (\theta) = \frac{Ellipticity\ (mdeg) \times 10^6)}{length\ (mm) \times Concentration(\mu M) \times Peptide\ bond\ number}$$

$$Helical\ Contents\ (\%) = \frac{MRE\ (\theta)_{222}}{Max(\theta)_{222}} \times 100\%$$

	$MRE\ (\theta)_{222}$	$Max(\theta)_{222}$	Helix contents
Ac-LK (7,11) (No Azo)	-12640.1	-36000	35 %
Ac-LK (7,11)-AB trans	-13873.6		31 %
Ac-LK (7,11)-AB UV	-20281.2		49 %
Ac-LK (7,11)-AB Vis	-15491.6		35 %
Ac-LK (7,11)-AB UV	-20824.3		50 %
Ac-LK (7,11)-AB Vis	-14784.9		33 %

Figure 8. CD spectral changes of acetylated Ab-LK(7,11) (100 μM in 50 mM PBS and 50% TFE) upon irradiation 365 nm and 440 nm, respectively.

3.8 FACS analysis for peptide penetration

HeLa (human cervical cancer), CHO-K1 (Chinese hamster ovary), HEK 293T (human embryonic kidney) or MDA-MB-231 (human breast cancer) were seeded at 24-well plates in DMEM medium supplemented with 10% FBS at a cell density of 100,000 cells/well. After 24 h incubation, the culture medium was replaced with fresh medium with 10% FBS. A stock solution (1 μM in 1 mL of deionized water) of TAMRA-labeled Ab-LK (7,11) peptide was prepared in a vial in the dark. An aliquot (500 μL) of the solution was transferred and irradiated UV for *cis* conformation with a 100W high-pressure mercury lamp (Lichtzen, South Korea) equipped with fiber optics and a 357 nm band-pass filter (Edmund optics, US). Each TAMRA-labeled peptide solution was diluted to a certain concentration with the DMEM (10% FBS) and treated to the cells. After 2 h incubation at 37° C, the medium was removed and cells were rinsed three times with PBS. Cells were then incubated with trypsin-EDTA for 5 min and detached from the wells. The detached cells were collected by centrifugation at 1,500 rpm. The collected cells were re-suspended in 500 μL PBS containing 2% FBS. The cellular uptake of the TAMRA-labeled peptides was analyzed by FACS Aria II (Becton Dickinson, Mountain View, CA).

The value of fluorescence-positive (+) cells (%) was defined as the percentage of TAMRA-(+) cells among all counted cells (10,000 cells) within a pre-fixed gate region. Triplicate experiments were performed for each sample.

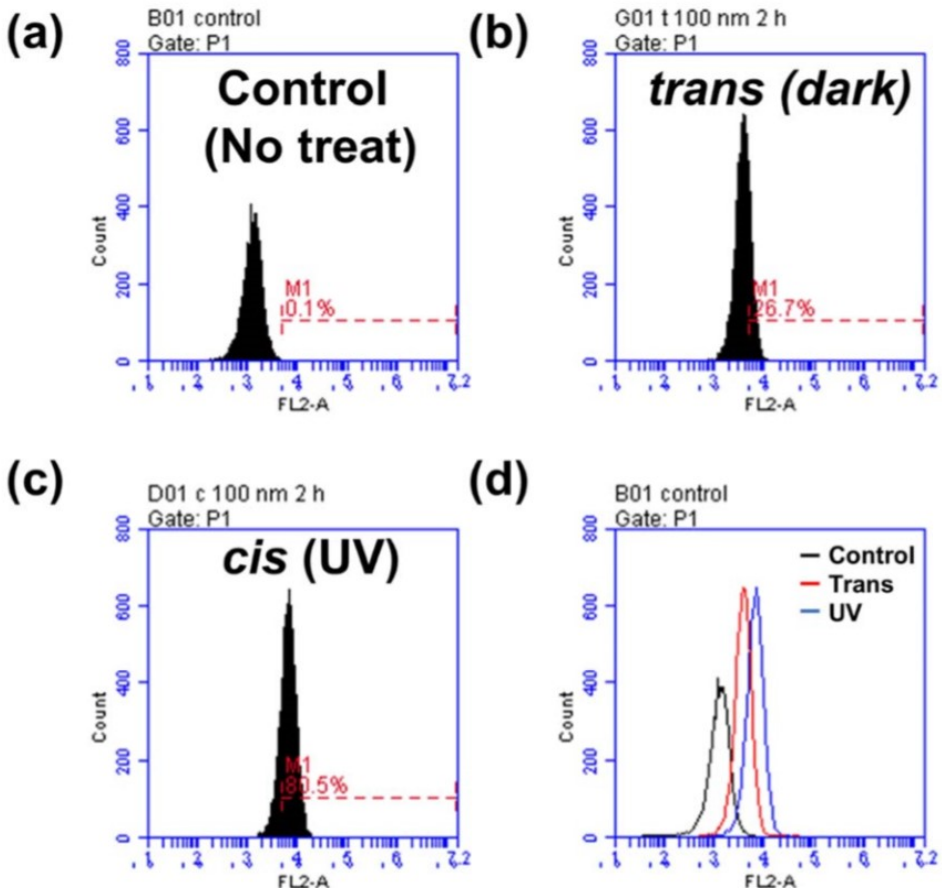

Figure 9. FACS results for 100 nM of Tamra Ab-LK (7,11) in HeLa cells. Each histogram plots a TAMRA fluorescence intensity (horizontal axis) against the number of events detected (vertical axis) and represents (a) control, (b) in the dark *trans*-Ab-LK, (c) UV-irradiated *cis*-Ab-LK, and (d) integrated form.

3.9 Confocal Laser Scanning Microscopy (CLSM)

HeLa cells (human cervical cancer cells) (5,000 cells/well) were cultured in 300 μL of DMEM supplemented with 10% FBS on 35-mm glass-base dishes (SPL Lifescience, South Korea) at 37° C in humidified 5% CO2 incubator. After 24 h incubation, the culture medium was exchanged with fresh medium with 10% FBS and each TAMRA-labeled Ab-LK peptide (200 nM) was added to the dish. After incubation for 4 h, cell nuclei are stained with a Hoechst 33342 solution (4 μM) for 30 min prior to the CLSM imaging. Cells were washed three times with PBS for the removal of peptides outside the cells, and fresh medium was added. CLSM images were acquired using a Zeiss DE/LSM 510 NLO (Carl Zeiss, Germany) with 500× objective (C-Apochromat, Carl Zeiss).

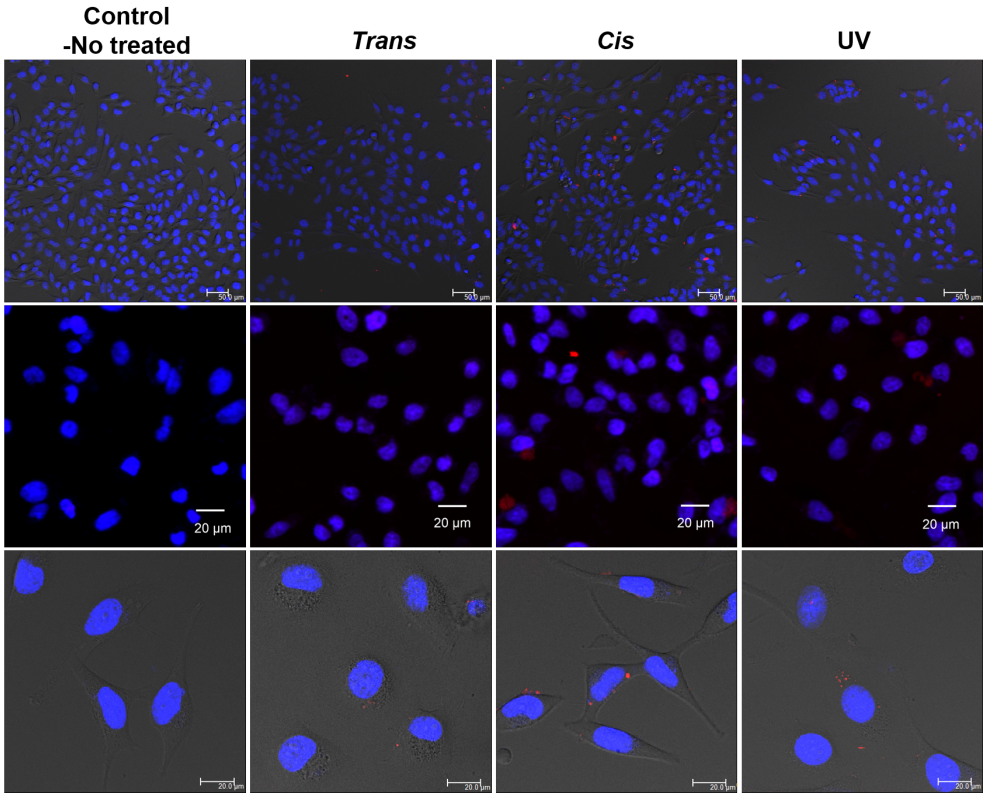

Figure 10. CLSM images of HeLa cells after 4 h treatment of each Tamra-labeled Ab-LK at 200 nM. Nucleus was stained with Hoechst 3342 (blue).

3.10 Dynamic Light Scattering (DLS)

Measurements of DLS spectra were performed using a Zetasizer (Malvern, Zetasizer Nano ZS) with a disposable solvent resistant micro cuvette (Malvern, ZEN0040). A stock solution (1 μM in 50 mM phosphate buffer solution (PBS) at pH 7.4) of acetylated Ab−LK (7,11) peptide was prepared in a vial in the dark. An aliquot (400 μL) of the solution was transferred to a cuvette and size was measured for the *trans* isomer. After measurement, the solution was irradiated UV light for 5 min, which resulted in *trans* to *cis* isomerization. Irradiation was carried out using a 100 W high−pressure mercury lamp (Lichtzen, South Korea) equipped with fiber optics and a 357 nm band−pass filter (Edmund optics, US). Size of *cis* isomer was recorded and then solution was re−irradiated by the lamp equipped with a 440 nm band−pass filter for 10 min for turning back to *trans* conformation. These irradiation UV/Vis cycles were repeated twice.

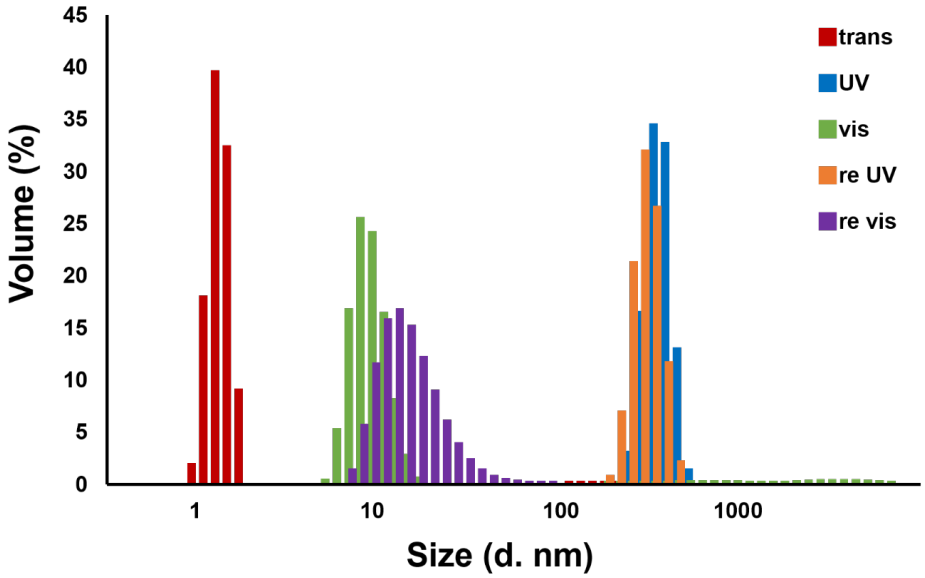

Figure 11. Size distribution curves obtained from DLS data of Acetylated Ab-LK(7,11) (1 μM in PBS solution). Peak shift from *trans* isomer (red) to a larger particle diameter with UV irradiated *cis* isomer (blue). Vis irradiation returning into *trans* isomer decreases the particle size (green) and re-irradiation UV (orange) and Vis (purple) were performed as repeated cycles.

3.11 Cytotoxicity assay

HeLa cells (human cervical cancer cells) (5,000 cells/well) were seeded at 94-well plates in 100 μL of DMEM medium containing 10% FBS for 24 h. After replacing the medium with fresh medium with 10% FBS, each diluted with the DMEM 10% FBS TAMRA-labeled Ab-LK peptide treated to the cells. After 2 h incubation at 37° C, the medium was removed and cells were rinsed three times with DMEM 10% FBS. 100 μL of CCK-8 solution (10 μL in 1 mL of medium) was then added to each well and incubated for an hour. The medium was removed from the wells and 100 μL of fresh DMEM medium containing 10% FBS was added. Absorbance was measured at 450 nm using a microplate reader (Molecular Devices Co., Menlo Park, CA, USA) and cell viability was calculated by comparison with untreated control cells.

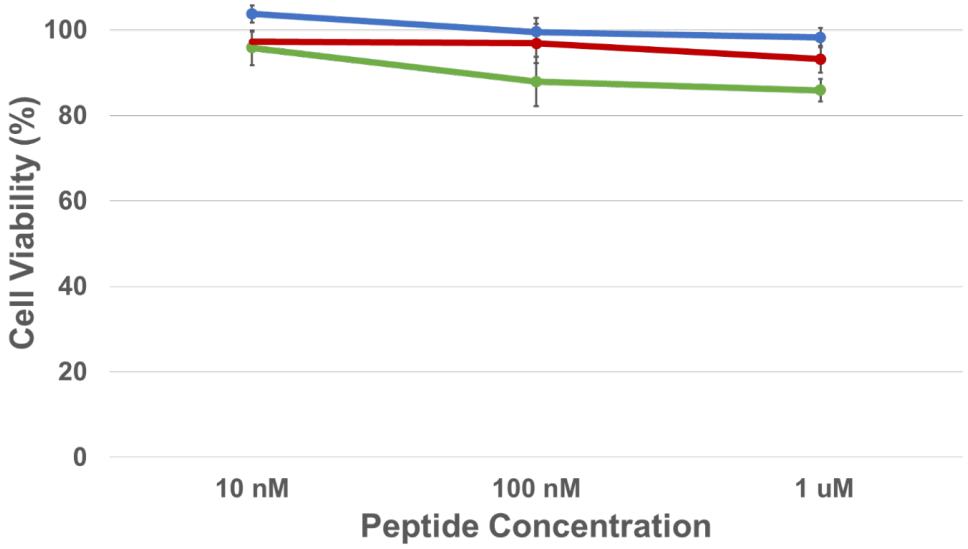

Figure 12. Relative viability of HeLa cells after 2 h treatment with each TAMRA-labeled Ab-LK at 10, 100 and 1000 nM. Each error bar represents the standard deviation (n = 3). UV-irradiated Ab-LK peptide (blue), in the dark Ab-LK peptide (red), and non Ab-stapled LK peptide (green) show not very toxicity on HeLa cells at these concentrations.

4. Results and Discussion

4.1 Preparation of the Ab-stapled LK peptide

Ab compound with two chloro-acetyl functional groups on each para-positions of diazophenyl rings for coupling with thiol residues of cysteines were prepared. The synthetic scheme is shown in Scheme 1. The Ab compound existed as the thermodynamically stable *trans* isomer (>98%) under ambient conditions in the dark (Figure 1). UV irradiation (λ_{max} = 365 nm) led to a photo-stationary state with the *cis* isomer as the major component (79%). We intended to turn on the cell-penetrating activity of the LK peptide by stabilizing of the α-helical conformation when a light signal is focused on the target site. To minimize the basal cell-penetrating activity without irradiation, we decided to disrupt the α-helix with the *trans*-state and to stabilize it with the *cis* state considering the maximal isomerization degrees of both states (98% vs 79%).

Ab-stapling at *i* and *i*+4 positions of α-helical peptides would be effective for conformational stabilization at the *cis* state because the α-helical pitch is 5.4Å, which is in accordance with the distance between the *para*-substituents of the *cis* state of the

Ab linker.[19] Among the 16 amino acids in the LK peptide (LKKLLKLLKKLLKLAG), two hydrophobic leucines were selected to be replaced with cysteines for the Ab stapling to minimize the change of total peptide hydrophobicity after the introduction of hydrophobic Ab moiety. In addition, because Ab stapling can induce the most dramatic helical conformational changes when it is incorporated in the middle of peptide sequences,[20] cysteines are introduced at the 7^{th} and 11^{th} positions of the LK sequence (LKKLLKCLKKCLKLAG) (**Figure 13**). Based on the rationales, Ab-stapled LK peptide (Ab-LK) was prepared by the coupling reactions between the Ab compound and the cysteines in the latter LK peptide (**Scheme 2**). The peptides were prepared by the standard Fmoc-based solid phase synthesis and purified using HPLC. Their molecular weights were confirmed using MALDI-TOF (**Figure 2-6**).

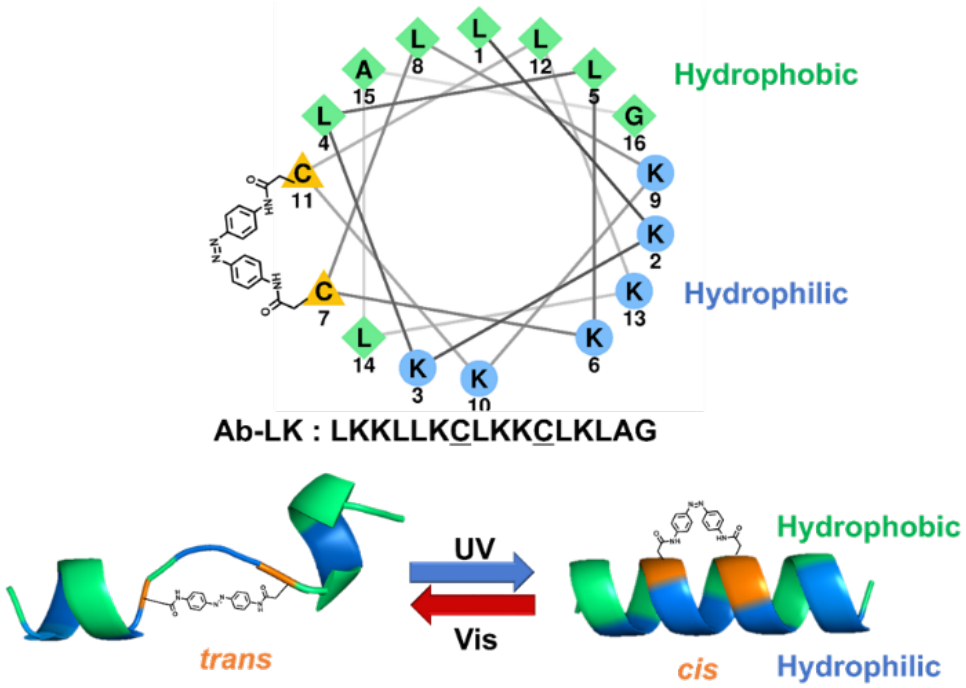

Figure 13. The wheel diagram of the Ab-stapled LK peptide (Ab-LK) and the conceptual scheme for photo-switching of the α-helical structure.

4.2 Photo-induced conformational change of the Ab-LK peptide

The photo-induced isomerization of Ab moieties in the Ab-LK peptide was examined by UV/Vis spectrometry (**Figure 7**and **Figure 14a**). Upon 1 min UV irradiation (λ_{max} = 365 nm) on the Ab-LK peptide, the strong $\pi-\pi*$ absorption band at approximately 360 nm was significantly reduced, whereas the weak $n-\pi*$ absorption band at approximately 450 nm was slightly increased. The spectral change is a characteristic phenomenon of the trans-cis Ab conversion.[21] Conversely, the initial spectrum was mostly recovered by Vis irradiation (λ_{max} = 445 nm) for 5 min, indicating that the Ab moiety gets reversibly isomerized even in the Ab-LK peptide structure. The change in the helical conformation of the Ab-LK peptide was analyzed by Circular Dichroism (CD) in PBS (**Figure 8**) and in 50 % PBS/TFE (**Figure 14b**). In general, the helix formation of Ab-LK was significantly enhanced in 50% PBS/TFE, showing higher α-helicities (35-56%) than those in PBS (19-24%). The membrane-mimicking condition (50% PBS/TFE) can stabilize the helical structure of many amphipathic peptides.[22] However, in both conditions, the UV irradiated Ab-LK represented increase in α-helicity. As shown in **Figure 14b**,

compared with the non-stapled LK peptide with an α-helicity of 35%, the trans form of Ab-LK peptide represented insignificantly different α-helicity (38%), whereas the UV-induced cis form of Ab-LK peptide represented remarkable increase in α-helicity (56%). Stapled α-helical peptides generally show higher α-helicity than non-stapled ones because of their lower degree of freedom.[23] The *i* and *i*+4 stapling with a too long trans Ab linker had a negligible effect on the stabilization of the α-helical conformation. On the contrary, the cis Ab stapling with an appropriate length could significantly stabilize the α-helical conformation. The choice of the Ab stapling points on the LK peptide was successful in inducing a notable change in the α-helical conformation. **Figure 14c** represents the reversible control of α-helicity by serial UV-Vis irradiation. Slightly higher α-helicity (41%-43%) of the Vis-irradiated samples than the initial α-helicity (38%) of 100% trans form might be due to the only 70% recovery of the trans form by the short irradiation for 5 min (**Figure 14d**). In summary, the results indicated that the α-helical secondary structure of the amphipathic peptide could be effectively and reversibly regulated by mild light signals (8 and 5 mW/cm2 for UV and Vis, respectively) with short durations.

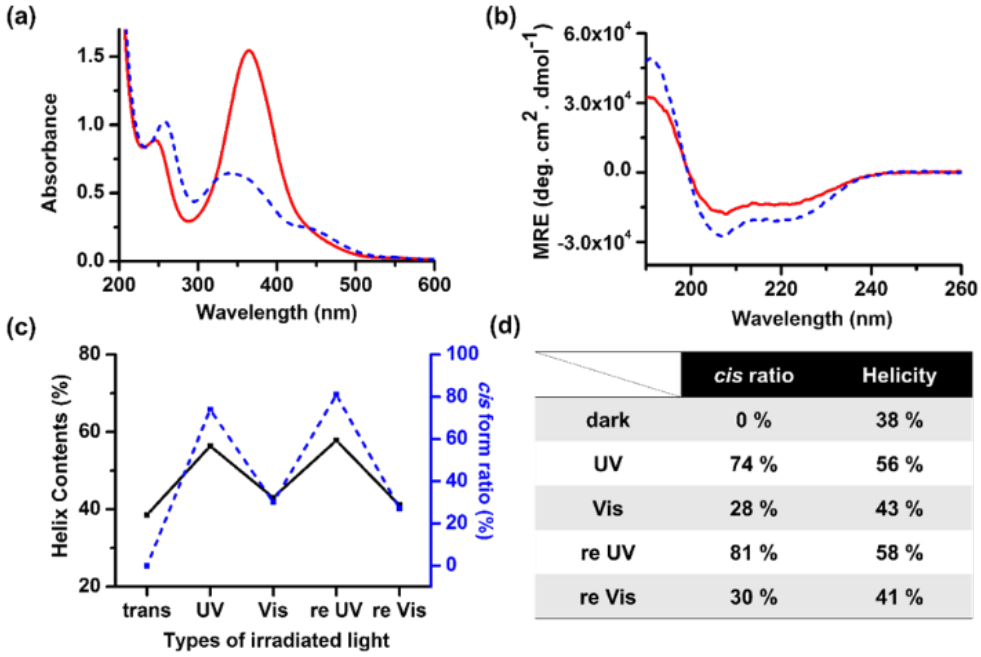

	cis ratio	Helicity
dark	0 %	38 %
UV	74 %	56 %
Vis	28 %	43 %
re UV	81 %	58 %
re Vis	30 %	41 %

Figure 14. Reversible photo-switching of the Ab-LK peptide. Solid red and dashed blue lines indicated the data from UV- and Vis-irradiated Ab-LK peptides, respectively. (a) UV/Vis spectra, (b) Circular Dichroism (CD) spectra of the Ab-LK peptide. (c) α-Helical change (black solid) and cis ratios (blue dash) of Ab-LK peptide by serial UV-Vis irradiation. (d) Summary of *cis* ratios and α-helicities of the Ab-LK peptide upon UV-Vis irradiation. The CD spectra were measured in phosphate buffer solution (50 mM, PBS pH 7.4) with 50% 2,2,2-trifluoroethanol (TFE) at room temperature.

4.3 Photo-switching of cell penetrating activity of the Ab-LK peptide

We compared the cell-penetrating activities on HeLa cells (human cervical cancer cells) between two isomeric forms by using *N*-terminal tetramethylrhodamine (TAMRA)-labeled Ab-LK peptide. Fluorescence-activated cell sorting (FACS) analysis represented the percentage of the TAMRA-positive cells (**Figure 15a**). After 2 h incubation, the LK peptide without Ab stapling showed only limited penetration (approximately 15%) at 100 nM, irrespective of the UV irradiation. However, the Ab-LK peptide showed a dramatic change in cell-penetrating activities responding to UV light. At 100 nM, non-irradiated Ab-LK peptide with mostly *trans* forms showed only 27% of TAMRA-positive cells, whereas UV-irradiated Ab-LK peptide mainly in the *cis* form showed 76% TAMRA-positive cells. In this submicromolar concentration, Tat peptide, the standard CPP, showed almost no TAMAR-positive cells. The comparison of mean fluorescence intensity (MFI) values also supported the clear activation of cell penetrating activity of the Ab-LK peptide by the UV irradiation (**Figure 15b**). The red fluorescence of the TAMRA-labeled Ab-LK peptide upon UV irradiation was observed in the confocal laser scanning microscopic

(CLSM) image (**Figure 15c**). We also observed *in situ* activation of cell penetration of the Ab-LK peptide by direct UV irradiation for 5 min on the cells. In a previous report, Möller's group showed that cell penetrating activity of oligo-arginines could be controlled by photo-irradiation.[24] They used charge-neutralization of cationic residues through *cis-trans* conversion of an Ab-linker for the penetration control at micromolar concentrations. However, in this research, we have shown that the cell penetrating activity can be effectively turned on at submicromolar concentrations by the UV-induced helix stabilization without any charge neutralization.

We also compared the cell permeability of Ab-LK on different cell types; CHO-K1 (Chinese hamster ovary cells), HEK 293T (human embryonic kidney cells) and MDA-MB-231 (human breast cancer cells) (**Figure 16**). Similar enhancement of cell permeability by UV-irradiation was observed in HEK 293T and MDA-MB-231 cells. However, the penetrating activity was lower and the UV-induced enhancement of the penetration was minimal in CHO-K1 cells which represented immature heparan sulfate proteoglycan (HSPG) receptors on the cell surface.[25] This result suggested a hypothesis that the Ab-LK could be internalized into cells via mediation of HSPG.[26]

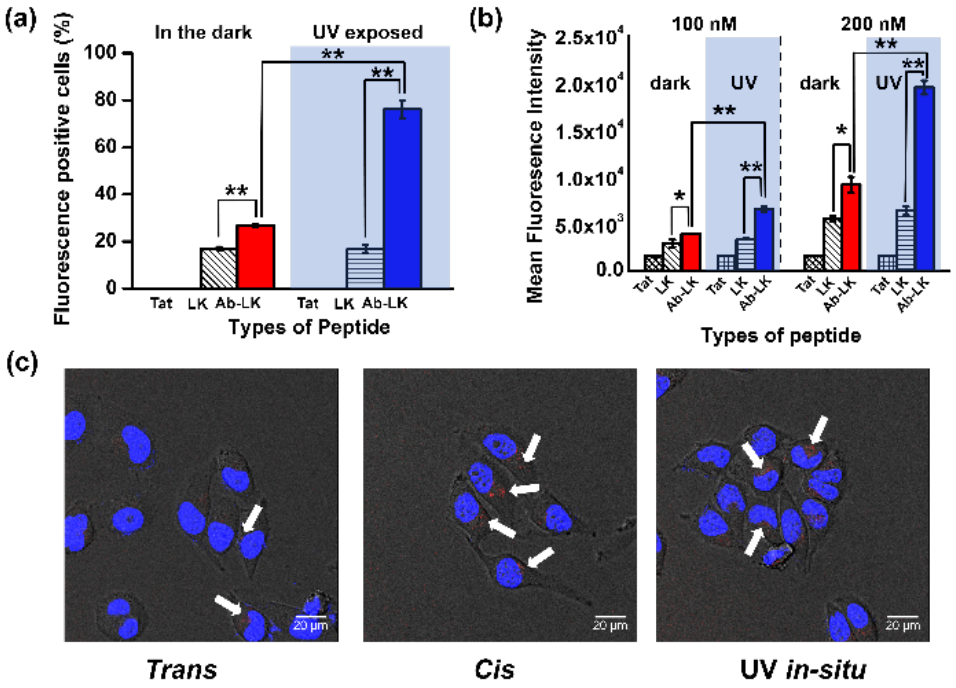

Figure 15. Photo-switching of cell penetration of the Ab-LK peptide on HeLa cells. (a) Percentage of fluorescence-positive cells after 2 h incubation with various TAMRA-labeled cell-penetrating peptides at 100 nM. (b) Mean fluorescence intensity (MFI) of HeLa cells treated with various TAMRA-labeled cell-penetrating peptides for 2h. Each error bar represents the standard deviation (n = 3). The markers (*) and (**) indicate $p < 0.05$ and $p < 0.01$, respectively. (c) CLSM images of HeLa cells treated with TAMRA-labeled (red) *trans* Ab-LK, *cis* Ab-LK,,and trans-Ab-LK in situ irradiated by UV for 5 min. The nucleus was stained with

Hoechst 33442 (blue). White arrows indicate TAMRA fluorescence signals (red) in the figure.

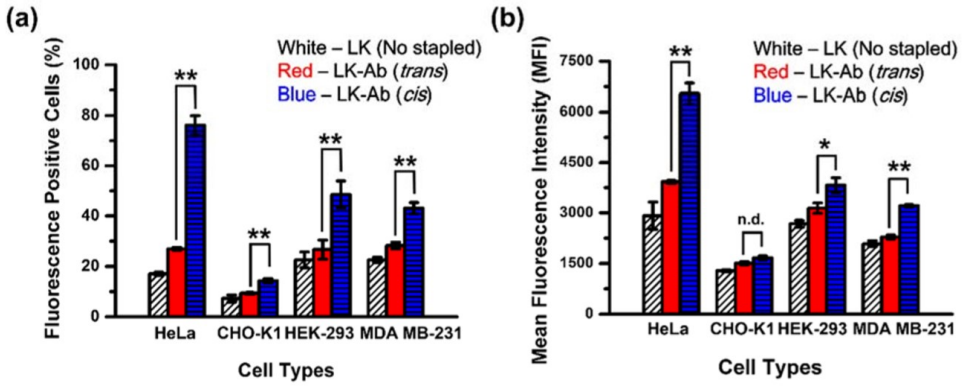

Figure 16. FACS results for 100 nM of Tamra Ab-LK (7,11) in various cell lines; HeLa, CHO-K1, HEK 293T, and MDA-MB-231. Tamra LK (white), non-irradiated Tamra Ab-LK (7,11) (red), and UVirradiated Tamra Ab-LK (7,11) (blue) were treated on the cell lines for 2 hours. (a) Percentage of fluorescence-positive cells and (b) mean fluorescence intensity (MFI) of peptide-treated cells. Each error bar represents the standard deviation (n = 3). The markers (*), (**) and (***) indicate $p < 0.05$, $p < 0.01$, and $p < 0.001$, respectively.

4.4 Photo-switching of association behaviors of the Ab-LK peptide

In order to understand reasons for the UV-activated cell penetrating activity of Ab-LK in more detail, we analyzed the association characteristics of the Ab-LK peptide in aqueous solutions. Interestingly, colloidal behavior of the Ab-LK peptide was greatly affected by the UV-Vis irradiation (Figure 17a). The *trans* Ab-LK and non-stapled LK peptide existed as a monomeric state with a diameter of 1.5 nm in the phosphate buffer (pH 7.4) (Figure S11). However, the UV-irradiated Ab-LK peptide rapidly formed associated structures of approximately 300 nm. The large difference in hydrodynamic diameters indicated that the association number of *cis* Ab-LK was significantly higher than *trans* Ab-LK. On the other hand, Vis re-irradiation on the UV-irradiated samples induced rapid dissociation to much smaller structures of approximately 10 nm. The photo-switched association-dissociation behavior of the Ab-LK peptide was reversible, as shown in the size change of the Ab-LK peptide that was serially irradiated by UV and Vis. It was clearly observed that the stabilization of the α-helix in the *cis*-Ab-LK peptide could have a strong potential in inducing multimeric structures through interactions between helices.

The reversible and dramatic change in the peptide associated structures suggested a mechanistic clue for elucidating the clear activation of cell penetration upon irradiation (**Figure 17b**). It was reported that cell internalization of CPPs was significantly dependent upon the associated structure.[27] Oligomeric or multimeric CPPs on cell surfaces could induce various cell penetration mechanisms.[28] The α-helix of non-stapled LK or non-irradiated Ab-LK peptides could not be effectively stabilized, and the cationic lysine-rich sequences with relatively free conformations were well hydrated and existed as the monomeric state. Conversely, *cis* Ab stapling through UV irradiation could stabilize the α-helix with well-defined cationic and hydrophobic faces, which successively formed larger multimeric structures by hydrophobic interaction between the peptide molecules. Particles with multi-positive charges over a critical size could effectively induce the endocytosis or direct penetration on the cell surfaces,[29] resulting in significant enhancement of cell-penetrating activities.

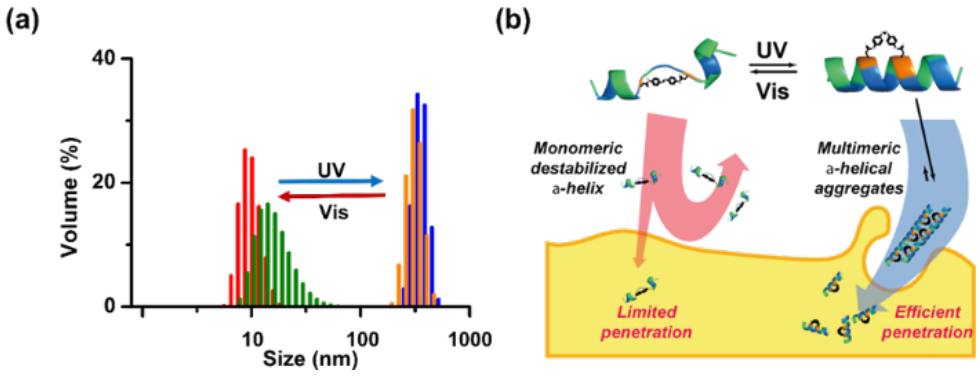

Figure 17. Photo-switching of association-dissociation of the Ab-LK peptide and entry to cells. (a) Dynamic laser light scattering (DLS) size distributions of *trans* Ab-LK (red and green) and *cis* Ab-LK (blue and orange) (b) A proposed mechanism of photo-switched cell penetration of the Ab-LK peptide.

4.5 Cytotoxicity and stability of the Ab-LK peptide

The Ab-LK peptide showed no significant cytotoxicity up to 1 μM on HeLa cells, far higher than the penetrating concentration (Figure 11). The large difference between the concentrations showing effective penetration and cytotoxicity supported that the Ab-LK system can have a potential to be used as a spatiotemporally controllable delivery carrier for hardly penetrable pharmaceuticals in the biological system. Additionally, we checked the stability of Ab-LK peptide against protease attack.[30] The Ab-LK peptide was degraded by trypsin (1 wt %), however, the degradation was significantly slower than the non-stapled LK peptide (Figure 18). Remarkably, the stapled part (CLLKCLK) of the LK sequence was stable even after the severe trypsin digestion. This result supported that the Ab-stapling can improve the serum stability of helical peptides, which would be important for the development of future peptide-based drugs.

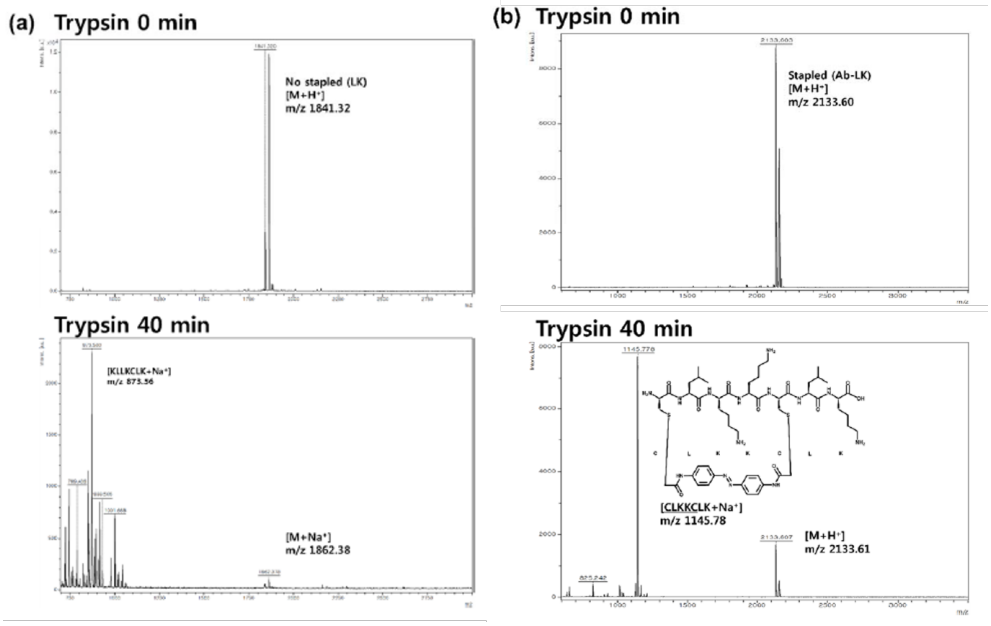

Figure 18. Stability of non-stapled LK and Ab-LK after treatment with trypsin (1 wt %). Nonstapled LK and Ab-LK (1 mg/mL) were treated by 1 wt % of trypsin in a 50 mM Tris-HCl buffer (pH 8.0). After incubation at 37°C, the samples were analyzed by MALDI-TOF. (a) Non-stapled LK peptide and (b) stapled Ab-LK peptide.

5. Conclusion

In this study, it is demonstrated that cell-penetrating activities of peptides can be controlled by light-induced Ab isomerization. The cell-penetrating activity of the Ab-LK peptide can be effectively regulated by photo-switching of secondary structures. The α-helical conformation was selectively stabilized by UV-induced *cis* Ab stapling of the amphipathic LK peptide, and the stabilized α-helix showed clear enhancement of cell-penetrating activities compared with the *trans* Ab-LK peptide with the same amino acid sequence but only different secondary structure. The remarkable dependence of cell-penetrating activity on the secondary structure as well as the formation of multimeric structures might be important information for future development of highly cell permeable peptide-based pharmaceuticals. Furthermore, photo-switching of cell penetration would be an effective drug targeting strategy with outstanding spatiotemporal specificity. Near IR or two-photon-responsive moieties should be incorporated instead of Ab for the future practical biomedical application of photo-switchable CPPs.[31]

6. Reference

[1] (a) Craik, D. J.; Fairlie, D. P.; Liras, S.; Price, D. The Future of Peptide-based drugs. *Chem. Biol. Drug. Des* 2013, *81*, 136-147. (b) Fosgerau, K.; Hoffmann, T. Peptide Therapeutics: Current Status and Future Directions. *Drug Discov. Today* 2015, *20*, 122-128.

[2] Nord, F. F. Advances in Enzymology and Related Areas of Molecular Biology; Merrifield, R. B.; Wiley: Hoboken, NJ, 2006; p 221-296.

[3] Bruno, B. J.; Miller, G. D.; Lim, C. S. Basics and Recent Advances in Peptide and Protein Drug Delivery. *Ther. Deliv.* 2013, *4*, 1443-1467.

[4] Aldrich, J. V.; Patkar, K. A.; McLaughlin, J. P. Zyklophin, a Systemically Active Selective Kappa Opioid Receptor Peptide Antagonist with Short Duration of Action. *Proc. Natl. Acad. Sci. U. S. A.* 2009, *106*, 18396-18401.

[5] (a) Nill, T.; Ishii, F. Encapsulation Efficiency of Water-Soluble and Insoluble Drugs in Liposomes Prepared by The Microencapsulation Vesicle Method. *Int. J. Pharm.* 2005, *298*, 198-205. (b) Kristensen, M.; Birch, D.; Nielsen, H. M. Applications and Challenges for Use of Cell-Penetrating Peptides as Delivery Vectors for Peptide and Protein Cargos. *Int. J. Mol. Sci.* 2016, *17*, 185-202.

[6] Bera, S.; Kar, R. K.; Mondal, S.; Pahan, K.; Bhunia, A. Structural Elucidation of the Cell-Penetrating Penetratin Peptide in Model Membranes at the Atomic Level: Probing Hydrophobic

Interactions in the Blood–Brain Barrier. *Biochemistry* 2016, *55*, 4982–4996.

[7] Guidotti, G.; Brambilla, L.; Rossi, D. Cell–Penetrating Peptides: From Basic Research to Clinics. *Trends Pharmacol. Sci.* 2017, *38*, 406–424.

[8] Copolovici, D. M.; Langel, K.; Eriste, E.; Langel, Ü. Cell–Penetrating Peptides: Design, Synthesis, and Applications. *ACS Nano* 2014, *8*, 1972–1994.

[9] (a) Dom, G.; Shwa–Jackson, C.; Matis, C.; Bouffioux, O.; Picard, J. J.; Prochiantz, A.; Mingeot–Lexlercq, M–P.; Brasseur, R.; Rezsohazy, R. Cellular Uptake of Antennapedia Penetratin peptides is a two–step process in which phase transfer precedes a tryptophan–dependent translocation. *Nucleic Acids Res.* 2003, *31*, 556–561. (b) Yandek, L. E.; Pokorny, A.; Florén, A.; Knoelke, K.; Langel, Ü.; Almeida, P. F. F. Mechanism of the Cell–Penetrating Peptide Transportan 10 Permeation of Lipid Bilayers. *Biophys. J* 2007, *92*, 2434–2444. (c) Liu, C.; Tai, L.; Zhang, W.; Wei, G.; Pan, W.; Lu, W. Penetratin, a Potentially Powerful Absorption Enhancer for Noninvasive Intraocular Drug Delivery. *Mol. Pharmaceutics* 2014, *11*, 1218–1227.

[10] Shu, J. Y.; Huang, Y–J.; Tan, C.; Presley, A. D.; Chang, J.; Xu, T. Amphiphilic Peptide–Polymer Conjugates Based on the Coiled–Coil Helix Bundle. *Biomacromolecules* 2010, *11*, 1443–1452.

[11] (a) Kritzer, J. A. Stapled Peptides: Magic Bullets in Nature’s Arsenal. *Nature Chemical Biology* 2010, *6*, 566–567. (b) Walensky, L. D.; Bird, G. H. Hydrocarbon–Stapled Peptides: Principles, Practice, and Progress. *J. Med. Chem.* 2014, *57*,

6275−6288. (c) Lau, Y. H.; de Andrade. P.; Wu, Y.; Spring, D. R. Peptide Stapling Techniques Based On Different Macrocyclisation chemistry. *Chem. Soc. Rev.* 2015, *44*, 91−102.

[12] Verdine, G. L.; Hilinski, G. H. Stapled Peptides for Intracellular Drug Targets. *Methods Enzymol.* 2012, *503*, 3−33.

[13] Dietrich, L.; Rathmer, B.; Ewan, K.; Bange, T.; Heinrichs, S.; Dale, T. C.; Schade, D.; Grossmann, T. N. Cell Permeable Stapled Peptide Inhibitor of Wnt Signaling that Targets β−Catenin Protein−Protein Interactions. *Cell Chemical. Biology* 2017, *24*, 958−968.

[14] (a) Eiríksdóttir, E.; Konate, K.; Langel, Ü.; Divita, G.; Deshayes, S. Secondary Structure of Cell−Penetrating Peptides Controls Membrane Interaction and Insertion. *Biochim. Biophys. Acta* 2010, *1798*, 1119−1128. (b) Zhang, Q.; Tang, J.; Fu, L.; Ran, R.; Liu, Y.; Yuan, M.; He, Q. A pH−Responsive α−Helical Cell Penetrating Peptide−Mediated Liposomal Delivery System. *Biomaterials* 2013, *34*, 7980−7993. (c) Yang, J.; Tsutsumi, H.; Furuta, T.; Sakurai, M.; Mihara, H. Interaction of Amphiphilic α−Helical Cell−Penetrating Peptides with Heparin Sulfate. *Org. Biomol. Chem.* 2014, *12*, 4673−4681. (d) Yamashita, H.; Oba, M.; Misawa, T.; Tanaka, M.; Hattori, T.; Naito, M.; Kurihara, M.; Demizu, Y. A Helix−Stabilized Cell−Penetrating Peptide as an Intracellular Delivery Tool. *ChemBioChem* 2015, *17*, 137−140.

[15] (a) Dhammika Bandara, H. M.; Burdette, S. C. Photoisomerization in Different Classes of Azobenzene. *Chem. Soc. Rev.* 2012, *41*, 1809−1821. 1510. (b) Mart, R. J.; Allemann, R. K. Azobenzene Photocontrol of Peptides and Proteins. *Chem. Commun.* 2016, *52*, 12262−12277.

[16] (a) Kim, Y.; Philips, J. A.; Liu, H.; Kang, H.; Tan, W. Using Photons to Manipulate Enzyme Inhibition by an Azobenzene-Modified Nucleic Acid Probe. *Proc. Natl. Acad. Sci. U. S. A.* 2009, *106*, 6489-6494. (b) Schierling, B.; Noël, A-J.; Wende,W.; Hien, L .T.; Volkov, E.; Kubareva, E.; Oretskaya, T.; Kokkinidis, M.; Römpp, A.; Spengler, B.; Pingoud, A. Controlling The Enzymatic Activity of a Restriction Enzyme by Light. *Proc. Natl. Acad. Sci. U. S. A.* 2010, *107*, 1361-1366.

[17] (a) Kumita, J. R.; Smart, O. S.; Woolley, G. A. Photo-Control of Helix Content in a Short Peptide. *Proc. Natl. Acad. Sci. U. S. A.* 2000, *97*, 3803-3808. (b) Flint, D. G.; Kumita, J. R.; Smart, O. S.; Woolley, G. A. Using an Azobenzene Cross-Linker to Either Increase or Decrease Peptide Helix Content upon *Trans*-to-*Cis* Photoisomerization. *Chemistry & Biology* 2002, *9*, 391-397.

[18] Jang, S.; Hyun, S.; Kim, S.; Lee, S.; Lee, I-S.; Baba, M.; Lee, Y.; Yu, J. Cell-Penetrating, Dimeric α-Helical Peptides: Nanomolar Inhibitors of HIV-1 Transcription. *Angew. Chem. Int. Ed.* 2014, *53*, 10086-10089.

[19] Bellotto, S.; Chen, S.; Rebollo, I. R.; Wegner, H. A.; Heinis, C. Phage Selection of Photoswitchable Peptide Ligands. *J. Am. Chem. Soc.* 2014, *136*, 5880-5883.

[20] (a) Samanta, S.; Woolley, G. A. Bis-Azobenzen Crosslinkers for Photocontrol of Peptide Structure. *ChemBioChem* 2011, *12*, 1712-1723. (b) Ail, A. M.; Woolley, G. A. The Effect of Azobenzene Cross-Linker Position on The Degree of Helical Peptide Photo-Control. *Org. Biomol. Chem.* 2013, *11*, 5325-5331.

[21] Hamm, P.; Ohline, S. M.; Zinth, W. Vibrational Cooling After Ultrafast Photoisomerization of Azobenzene Measured by

Femtosecond Infrared Spectroscopy. *J. Chem. Phys.* 1997, *106*, 519−529..

[22] (a) Shiraki, K.; Nishikawa, K.; Goto, Y. Trifluoroethanol-induced Stabilization of the α-Helical Structure of β-Lactoglobulin: Implcation for Non-hierarchical Protein Folding. *J. Mol. Biol.* 1955, *245*, 180−194. (b) Myers, J. K.; Pace, C. N.; Scholtz, J. M. Trifluoroethanol Effects on Helix Propensity and Electrostatic Interactions in the Helical Peptide from Ribonuclease T_1. *Protein Sci.* 1998, *7*, 383−388.

[23] Grison, C. M.; Burslem, G. M.; Miles, J. A.; Pilsl, L. K. A.; Yeo, D. J.; Imani, Z.; Warriner, S. L.; Webb, M. E.; Wilson, A. J. Double Quick, Double Click Reversible Peptide "Stapling". *Chem. Sci.* 2017, *8*, 5166−5171.

[24] Prestel, A.; Möller, H. M. Spatio-Temporal Control of Cellular Uptake Achieved by Photoswitchable Cell-Penetrating Peptides. *Chem. Commun.* 2016, *52*, 701−704.

[25] (a) Xu, X.; Nagarajan, H.; Lewis, N. E.; Pan, S.; Cai, Z.; Liu, X.; Chen, W.; Xie, M.; Wang, W.; Hammond, S.; Andersen, M. R.; Neff, N.; Passarelli, B.; Koh, W.; Fan, H. C.; Wang, J.; Gui, Y.; Lee, K. H.; Betenbaugh, M. J.; Quake, S. R.; Famili, I.; Palsson, B. O.; Wang, J. The Genomic Sequence of the Chinese Hamster Ovary (CHO)-K1 Cell Line. *Nat. Biotechnol.* 2011, *29*, 735−741; (b) Zhang, L.; Lawrence, R.; Frazier, B. A.; Esko, J. D. CHO Glycosylation Mutants: Proteoglycan. *Methods Enzymol.* 2006, *416*, 205−221.

[26] (a) Christianson, H. C.; Belting, M. Heparan Sulfate Proteoglycan as a Cell-Surface Endocytosis Receptor. *Matrix Biol.* 2014, *35*, 51−55 (b) Sarrazin, S.; Lamanna, W. C.; Esko, J. D.

Heparan Sulfate Proteoglycan. *Cold Spring Harb Perspect. Biol.* 2011, *3*, 1−33.

[27] (a) Wadhwani, P.; Reichert, J.; Bürck, J.; Ulrich, A. S. Antimicrobial and Cell−Penetrating Peptides Include Lipid Vesicle Fusion by Folding and Aggregation. *Eur. Biophys. J.* 2012, *41*, 177−187. (b) Macchi, S.; Signore, G.; Boccardi, C.; Di Rienzo, C.; Beltram, F.; Cardarelli, F. Spontaneous Membrane−Translocating Peptides: Influence of Peptide Self−Aggregation and Cargo Polarity. *Sci. Rep.* 2015, *5*, 16914−16925.

[28] Kauffman. W. B.; Fuselier. T.; He. J.; Wimley. W. C. Mechanism Matters: A Taxonomy of Cell Penetrating Peptides. *Trends Biochem. Sci.* 2015, *12*, 749−764.

[29] (a) Trabulo, S.; Cardoso, A. L.; Mano, M.; de Lima, M. C. P. Cell−Penetrating Peptides−Mechanisms of Cellular Uptake and Generation of Delivery System. *Pharmaceuticals* 2010, *3*, 961−993. (b) Schmidt, N.; Mishra, A.; Lai, G. H.; Wong, G. C. L. Arginine−Rich Cell−Penetrating Peptides. *FEBS Lett.* 2010, *584*, 1806−1813.

[30] Olsen, J. V.; Ong, S−E.; Mann, M. Trypsin Cleaves Exclusively C−Terminal to Arginine and Lysine Residues. *MCP*. 2004, *3*, 608−614.

[31] Beharry, A. A.; Sadovski, O.; Woolley, G. A. Azobenzene Photoswitching without Ultraviolet Light. *J. Am. Chem. Soc* 2011, *133*, 19684−19687.

PART 2. Photo-Control of Beta-Sheet with Antimicrobial Activity of Arenicin-1

1. Abstract.

In order to develop more bacterial cell selective peptide, Arenicin-1 (AR-1), antimicrobial peptide isolated from marine lugworm *Arenicola marina*, were modified by photo-induced structure change for antimicrobial activity. It was reported that AR-1 adopts the twisted β-hairpin structure playing important role in high antibacterial activity with a single disulfide bond between Cys3 and Cys20. Those two Cystein (Cys, C) were stapled with an Ab linker, and the geometrical conversion of the Ab-linker by UV-Vis irradiation induced a remarkable change of the β-sheet conformation of the Ab-stapled AR-1 peptide (Ab-AR-1). However, their antimicrobial activities were slightly dependent upon the irradiation wavelengths, resulting that UV-induced *cis* Ab-AR-1 with a destabilized beta-sheet structure showed slightly recovered antimicrobial activity from Vis-induced *trans* Ab-AR-1.

Replacing Ab linker, *o*-nitrobenzyl (*o*-Nb) groups which can be cleaved by UV irradiation were applied to two Cys residues

on AR-1. Photo-caged AR-1 interrupted forming disulfide bridge in consequence less active against bacterial cells than original form of AR-1. Interestingly, upon UV-irradiated *o*-Nb-AR-1 recover their own antimicrobial activity resulting in de-protection of *o*-Nb group from the Cys residues on AR-1 and restored their β-sheet secondary structure.

2. Introduction.

Antibiotics agents are essential and widely used in the treatment of bacterial infectious diseases. However, the emergence of the drug resistance bacteria has become a major problem for general use of antibiotics.[32] Along with social awareness the necessary of decreasing the inappropriate use of antibiotics in modern health care, many efforts have been made to identify more potent and safe antibiotic agents.[33]

Antimicrobial peptides playing important role in the innate host defence mechanism are attractive candidates for new antibiotics.[34-36] Antimicrobial peptides are short 15-40 amino acid peptide that are capable of disrupting cell membranes, but fundamental structural principle underlying is adopting a shape in amphipathic manner with cationic and hydrophobic amino acids.[37-38] Arenicin-1 (AR-1: RWCVYAYVRVRGVLVRYRRCW), 21-residue antimicrobial peptide, was purified from coelomocytes of the marnie polychaeta *Arenicola marina* (lugworm).[39] This antimicrobial peptide contains a single disulphide bridge between Cys3 and Cys20, forming a large 18-reside ring.[39] AR-1 has two-stranded antiparallel β-sheet structures with antimicrobial activity,

however, it also displayed cytotoxicity against human red blood cells.[40] Hence, discrimination between eukaryotic and prokaryotic cell inducing minimal cytotoxicity toward the host cells is the one of the major obstacles and goals for development of new potent antibiotics.

Light is an attractive external trigger for the control of biological functions[41-42] because it offers highly spatiotemporal resolution, it is relatively non-invasive and biorthogonal, and it does not lead to sample contamination.[43] Furthermore, its intensity and wavelength can be regulated with very high precision.[44] Azobenzene (Ab) is a well-known photo-responsive moiety showing reversible *cis-trans* structural conversion responding to UV and Vis light.[45] The difference of the distance between the *para*-substituents in the Ab moieties (≈ 10Å) during the geometric conversion is sufficient for inducing large structural changes in peptides.[46] β-sheet conformations could be reversibly formed and deformed by photo-switching of Ab moieties that were conjugated to carefully selected amino acid residues.[47] These molecules undergo a light-induced change in their structure that results in a change in their properties. By introducing photoactive compounds

into biomolecules, these effects may be translated into changes in the functioning of biological system. Light-cleavable group, such as *o*-nitro benzyl group can protect thiol functional group of cysteine residues[48] and temporarily block forming disulphide bond on AR-1. Once irradiated by UV light, photo-cleavable groups were detached, the original of photo-caged peptide regained and recovered facilitated to original functions.[49]

To address the challenges associated with the emergence of bacterial resistance, take advantage of the special properties of light in anticipation that control of antimicrobial activity might be achieved by designing photo-responsive antibiotics. In order to design more effective antimicrobial peptide without haemolytic activity, photo-responsive Ab-AR-1 and *o*-Nb-AR-1 peptide were synthesized by introducing Ab and *o*-Nb groups on two cysteins respectively. The antimicrobial activity against bacteria of photo-responsive AMP is measured and their secondary structure change correlated with antimicrobial activity demonstrated selective activation upon light irradiation.

3. Experimental Section

3.1 Materials

All chemicals were purchased from commercial suppliers and used without further purification. 4, 4’ −Diaminoazobenzene was purchased form Alfa Asear (US) and chloroacetyl chloride was purchased from TCI (Japan). Triethylamine (TEA) was purchased form Aldrich (US) and sodium sulfate (Na_2SO_4) was purchased form Daejung (South Korea). Chloroform (CH_3Cl), dimethylforamide (DMF), dichloromethane (DCM) and hexane were purchased from Samchun Chemical (South Korea). *N*,*N*−dimethylformamide (DMF) were purchased from Sigma−Aldrich (St. Louis, MO, USA). 2−Nitrobenzyl bromide was purchased form TCI (Japan) and tris(2−carboxyethyl)phosphine hydrochloride (TCEP) was purchased form Alfa Asear (US). Arenicin−1 (AR−1) were purchased from ANYGEN (South Korea) and dimethylforamide (DMF) were purchased from Samchun Chemical (South Korea).

3.2 Synthesis of Azobenzne-diacetyl chloride

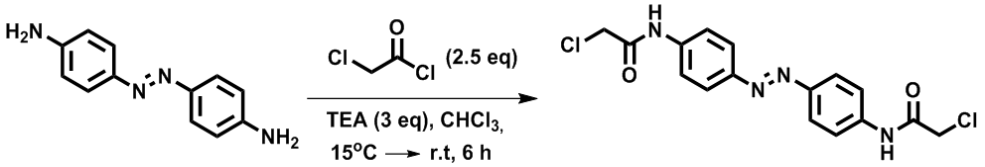

Scheme 2. Synthetic scheme of Ab-diacetyl chloride.

4,4'-Diaminoazobenzene (200 mg, 0.94 mmol) was dissolved in $CHCl_3$ (100 mL), then cooled to 15° C. Triethylamine (394 μL, 3 eq) was added and chloroacetyl chloride (187 μL, 2.5 eq) was added to the mixture. The mixture was stirred at room temperature for 6 h. The reaction was quenched by addition of water (100 mL). The organic layer was separated, washed with water twice (2 × 100 mL), dried over sodium sulfate (Na_2SO_4). The solvent was evaporated in vacuum to afford brown solid. The crude product was recrystallized in DMF/DCM/hexane (1:20:20) to yield yellow solid. 93% (320 mg). ^{1}H-NMR (500 MHz, DMSO-d_6, 298K, ppm) δ 10.64 (s, NH), 7.88 (d, J = 10.0 Hz, 2H), 7.81 (d, J = 10.0 Hz, 2H), 4.31 (s, 2H). ^{13}C-NMR (500 MHz, DMSO-d_6, 298K, ppm) 164.97, 148.01, 141.09, 123.40, 119.62, 43.54.

3.3 ^{1}H NMR spectra of Azobenzene linker

Stock solution (4 mM in DMSO-d_6) of Ab-diacetyl chloride was prepared in a vial in the dark. An aliquot (400 μL) of the solution was transferred to a NMR tube and ^{1}H NMR spectrum was recorded for the *trans* isomer. After the measurement, the solution was transferred to a quartz cell and irradiated UV light for 5 min, which resulted in *trans* to *cis* isomerization. Irradiation was carried out using a 100W high-pressure mercury lamp (Lichtzen, South Korea) equipped with fiber optics and band-pass filters (Edmund optics, US). For UV irradiation, a 357 nm band-pass filter with a 48 nm full width-half-max (FWHM) was used (OD > 6.0). ^{1}H NMR spectrum was recorded and the population of the cis isomer at the photo-stationary state (PSS' s) was determined by the ^{1}H NMR integration of each shifted signals.

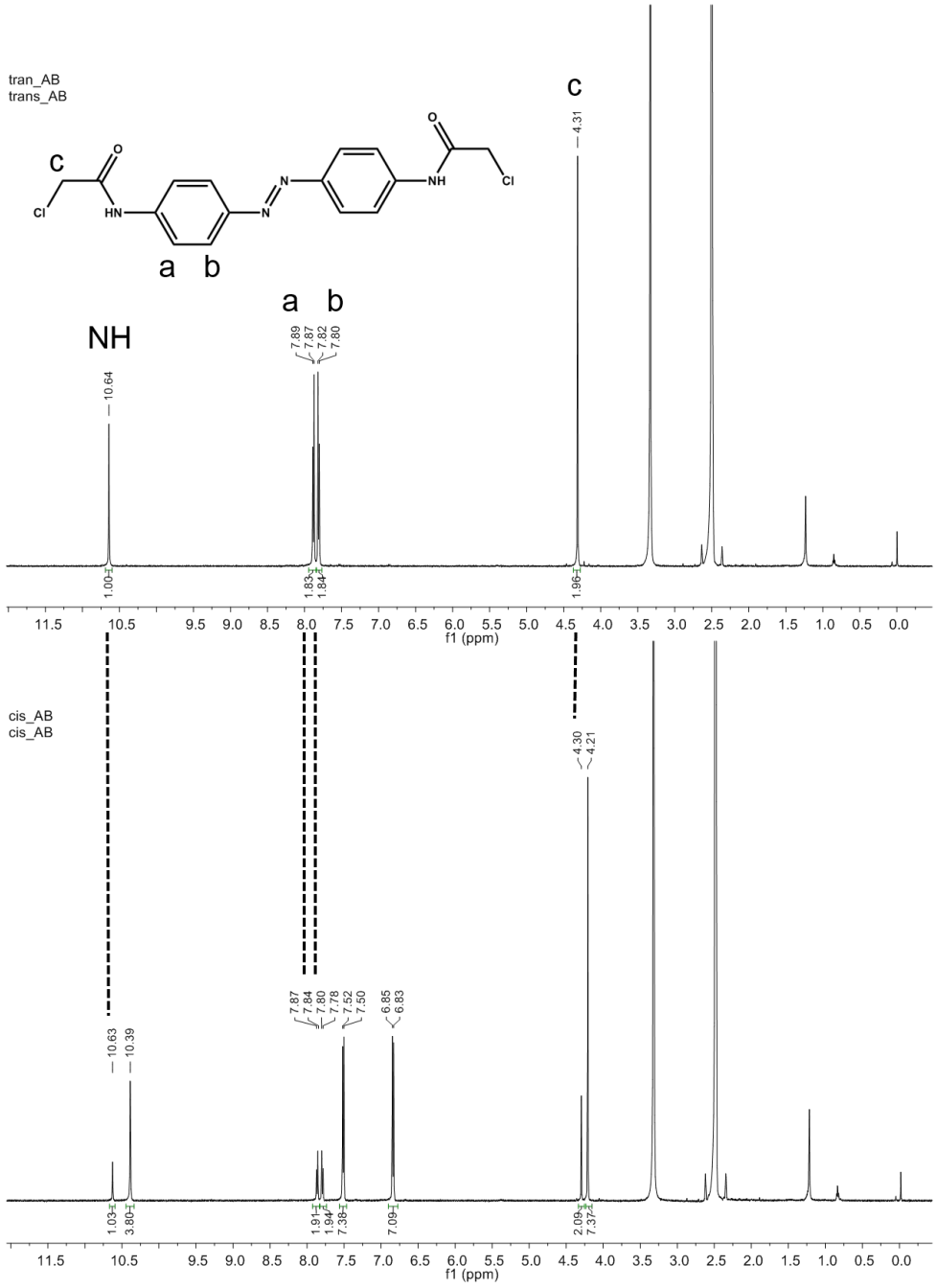

Figure 19. ^{1}H NMR spectra (500MHz, 4 mM in DMSO-d_6, 25℃) of Ab-diacetyl chloride. *Trans* isomer (top) and *cis* isomer (bottom); *trans* : *cis* = 21 : 79 at PSS.

3.4 Stapling of AR-1 with Azobenzene linker

Intramolecular stapling of the AR-1 peptide (sequence: RWCVYAYVRVRGVLVRYRRCW) was performed in the presence of guanidine hydrochloride (GdnHCl) to disrupt the secondary structure during the coupling reaction. The AR-1 peptide (0.5 mM) and tris(2-carboxyethyl)phosphine hydrochloride (TCEP) (1 mM) were dissolved in an aqueous solution containing 100 mM Tris-HCl and 8 M GdnHCl at pH 8.0. The reaction mixture was allowed to be stirred for an hour at ambient temperature. The synthesized Ab-diacetyl chloride (0.5 mM) was dissolved in DMF and the solution was mixed with the peptide solution. After 24 h-stirring, the stapled peptide (Ab-AR-1) was purified using HPLC with the same protocol described above.

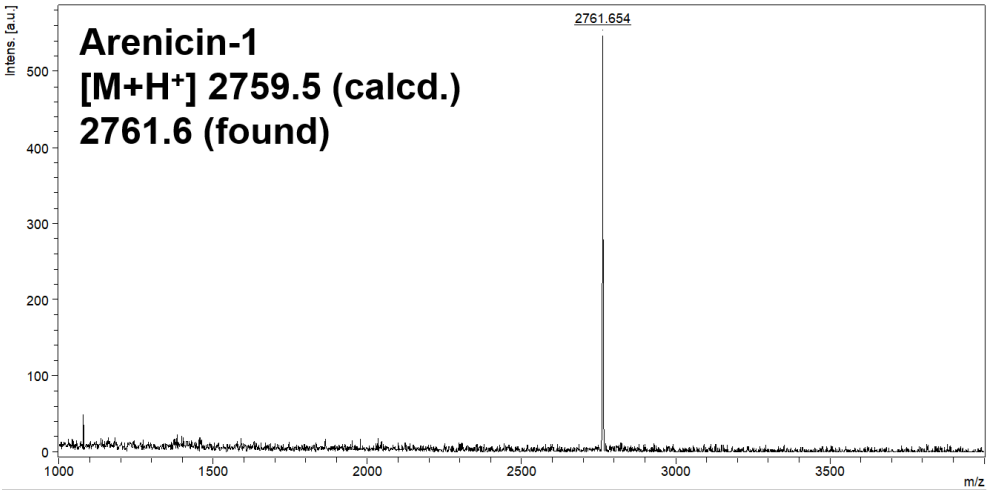

Figure 20. AR-1 (sequence: RWCVYAYRRVRGVLVRYRRCW) was obtained as white powder. MS ($M+H^+$) 2759.5 (calcd.), 2761.6 (found).

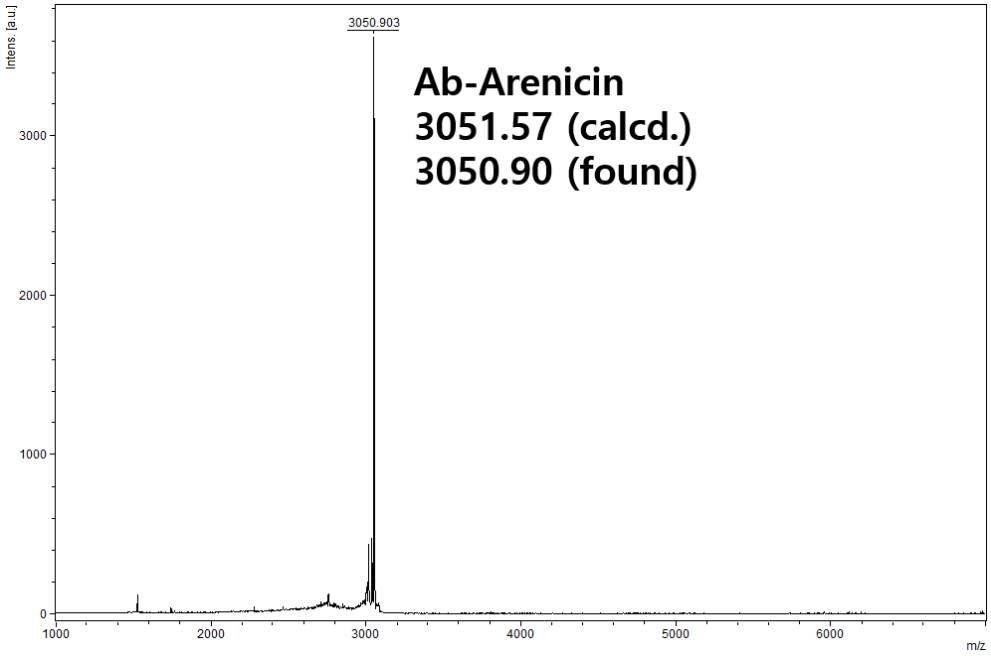

Figure21. Ab-AR (sequence: Ab-RWCVYAYRRVRGVLVRYRRCW) was obtained as yellowish powder. MS ($M+H^+$) 3051.6 (calcd.), 3050.9 (found).

3.5 Photo-induced UV/Vis spectral change

Measurements of UV/Vis absorption spectra were performed in a high precision quartz cell (Hellma Analytics) using a UV/Vis spectrophotometer (JASCO, V-650). Absorption was measured from 200 to 600 nm. Stock solution (25 μM in a 50 mM phosphate buffer solution (PBS) pH 7.4) of Ab-AR peptide was prepared in a vial in the dark. An aliquot (300 μL) of the solution was transferred to a UV quartz cell and UV/Vis absorption spectrum was recorded for the *trans* isomer. After measurement, the solution was irradiated UV light for 5 min, which resulted in *trans* to *cis* isomerization. Irradiation was carried out using a 100 W high-pressure mercury lamp (Lichtzen, South Korea) equipped with fiber optics and a 357 nm band-pass filter (Edmund optics, US). UV/Vis spectrum was recorded for the *cis* isomer and then solution was re-irradiated by the lamp with a 440 nm band-pass filter for 10 min for the recovery to *trans* conformation. These irradiation UV/Vis cycles were repeated twice and the population of the *cis* isomer at the photo-stationary state (PSS' s) was determined by the intensities of λ_{max} (365 nm) signals assuming that *trans* isomer exists as 100 % and the maximum changes would be the difference

between absorbance values at 365 nm for *trans* isomer and the background.

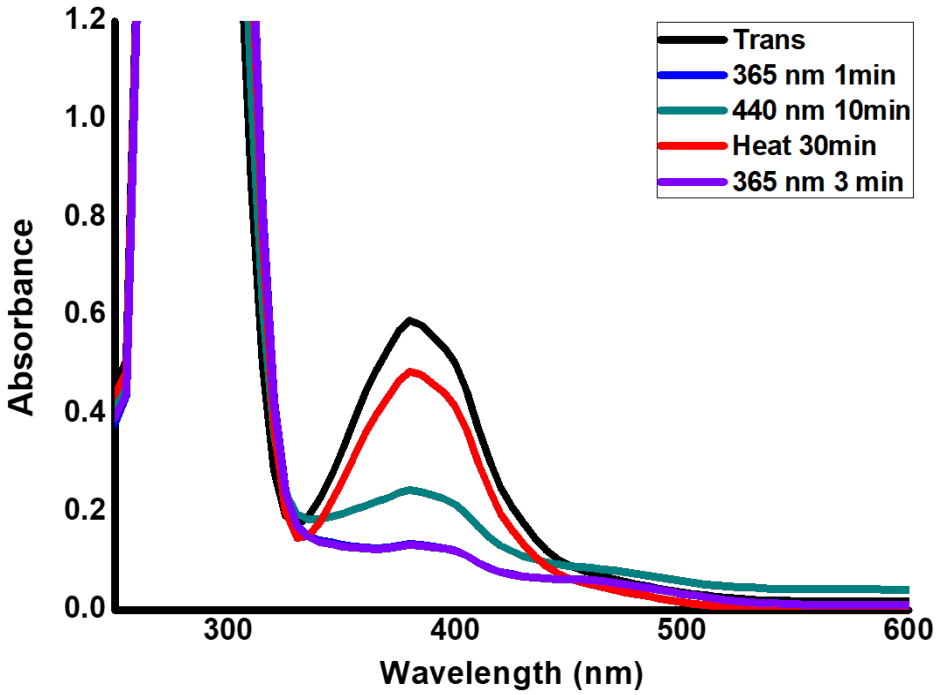

$$trans\ ratio\ (\%) = \frac{Abs_{measure}}{Abs_{trans}} \text{ x } 100\ (\%)$$

	$Abs_{380\ nm}$	*trans* : *cis*
Ab-AR-1 trans	0.58947	100 %
Ab-AR-1 UV (365 nm)	0.16599	28 % (72 %)
Ab-AR-1 Vis (440 nm)	0.24505	41 % (59 %)
Ab-AR-1 Heat (50 °C)	0.48014	82 % (18 %)
Ab-AR-1 UV (365 nm)	0.1329	22 % (78 %)

Figure 22. UV/Vis absorption spectral changes of Ab-AR-1 (25 μM in 50 mM PBS pH 7.4, 25℃) upon irradiation at 365 nm for 1, 3 min and 440 nm for 10 min, respectively.

3.6 Circular dichroism (CD)

Measurements of CD spectra were performed using a Circular Dichroism spectropolarimeter (JASCO, J-815) with a 1.0 mm path-length cell (JASCO). CD was scanned from 190 to 260 nm with a set-up of 0.2 s-integration, 1 nm-step resolution and 1 nm-bandwidth. The results from three scans were averaged. β-sheet of Ab-AR-1 peptide was measured in phosphate buffer solution (50 mM PBS pH 7.4) with 50% 2,2,2-trifluoroethanol (TFE) as a membrane-mimic condition at room temperature. A stock solution (50 μM in PBS and 50% TFE) of Ab-AR-1 peptide was prepared in a vial in the dark. An aliquot (300 μL) of the solution was transferred to a cell and the CD spectrum was recorded for the trans isomer. After measurement, the solution was irradiated by UV light for 5 min, which resulted in *trans* to *cis* isomerization. Irradiation was carried out using a 100W high-pressure mercury lamp (Lichtzen, South Korea) equipped with fiber optics and a 357 nm band-pass filter (Edmund optics, US). After record for the cis isomer and the solution was re-irradiated by the lamp equipped with a 440 nm band-pass filter for 10 min for *cis* to *trans* isomerization. These irradiation cycles were repeated twice and the change of β-sheet was calculated.

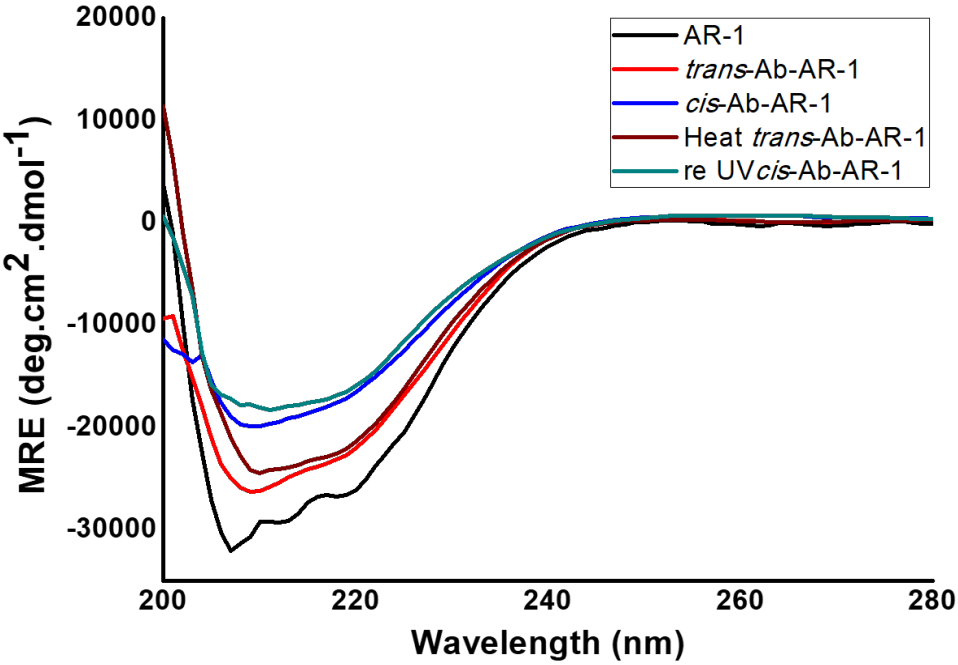

$$MRE\ (\theta) = \frac{Ellipticity\ (mdeg) \times 10^6)}{length\ (mm) \times Concentration(\mu M) \times Peptide\ bond\ number}$$

$$\beta\text{-sheet}\ Contents\ (\%) = \frac{MRE\ (\theta)_{218}}{Max(\theta)_{218}} \times 100\%$$

	$MRE\ (\theta)_{218}$	$Max(\theta)_{218}$	**θ-sheet contents**
AR-1 (No Azo)	-26743.2	-36000	74 %
trans Ab-AR-1	-23098		64 %
UV *cis* Ab-AR-1	-17592.9		49 %
Heat *trans* Ab-AR-1	-22536.2		63 %
re UV *cis* Ab-AR-1	-16860		47 %

Figure 23. CD spectral changes of AR-1 and Ab-AR-1 (100 μM in 50 mM PBS and 50% TFE) upon irradiation 365 nm for 5 min and 50℃ for 30 min, respectively.

3.7 Minimum inhibitory concentration (MIC) test

The antimicrobial activities of the peptides were examined in sterile 96-well plates in a final volume of 200 μL and the procedures are as follows. Briefly, aliquots (10 μL) of a bacterial suspension at 2×10^7 colony-forming units (CFU)/mL in Luria-Bertani (LB) broth were added to 180 μL of peptide solution (serial 2-fold dilutions in LB broth. After incubation for 18-20 h at 37 ℃, the inhibition of bacterial growth was determined by measuring the absorbance at 600 nm with a Micro plate auto reader EL 800 (Bio-Tek Instruments). The minimal inhibitory concentration (MIC) was defined as the lowest concentration of the peptide required to inhibit bacterial growth. Gram-negative bacteria (*Escherichia coli* [ATCC 25922] were purchased from the Korean Collection for Type Cultures (KCTC) at the Korea Research Institute of Bioscience and Biotechnology.

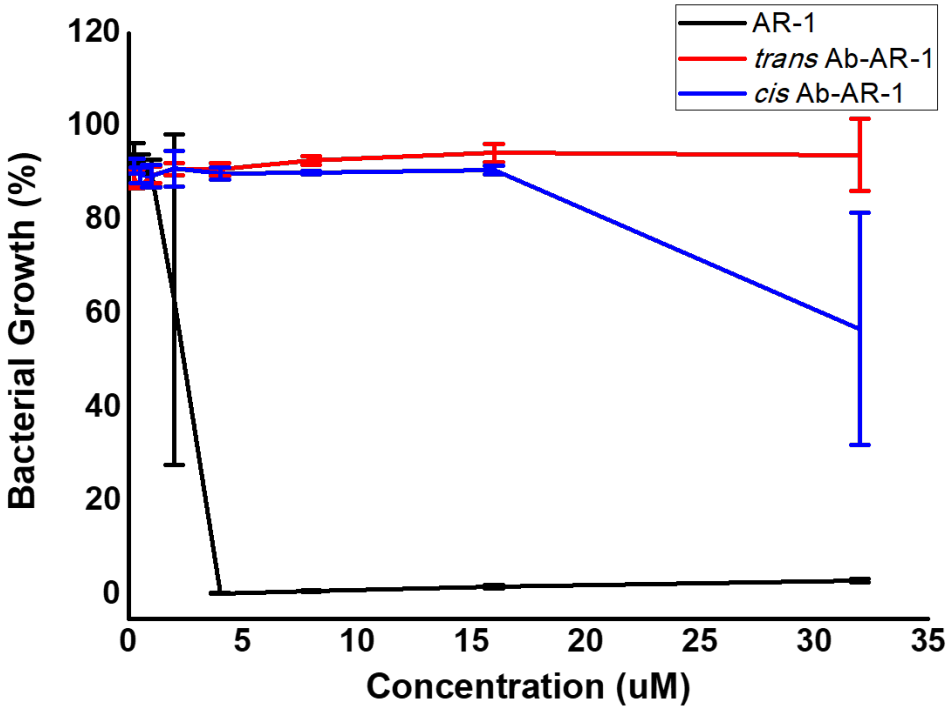

Figure 24. Bacterial growth spectrum depending on concentration of AR-1 and Ab-AR-1 (0.5 to 32 μM incubated for 20h at 37℃)were measured the absorbance at 600 nm.

4. Results and Discussion

4.1 Preparation of the Ab-stapled AR-1 peptide

Ab compound with two chloro-acetyl functional groups on each para-positions of diazophenyl rings for coupling with thiol residues of cysteines were prepared. The synthetic scheme is shown in Scheme 2. The Ab compound existed as the thermodynamically stable *trans* isomer (>98%) under ambient conditions in the dark (Figure 19). UV irradiation (λ_{max} = 365 nm) led to a photo-stationary state with the *cis* isomer as the major component (79%). Intended to turn on the antimicrobial activity of the Arenicin-1 (AR-1) peptide by stabilizing of the β-sheet conformation when a light signal is focused on the target site. To minimize the basal antimicrobial activity without irradiation, it is decided to disrupt the β-sheet with the *trans*-state and to stabilize it with the *cis* state considering the maximal isomerization degrees of both states (98% vs 79%).

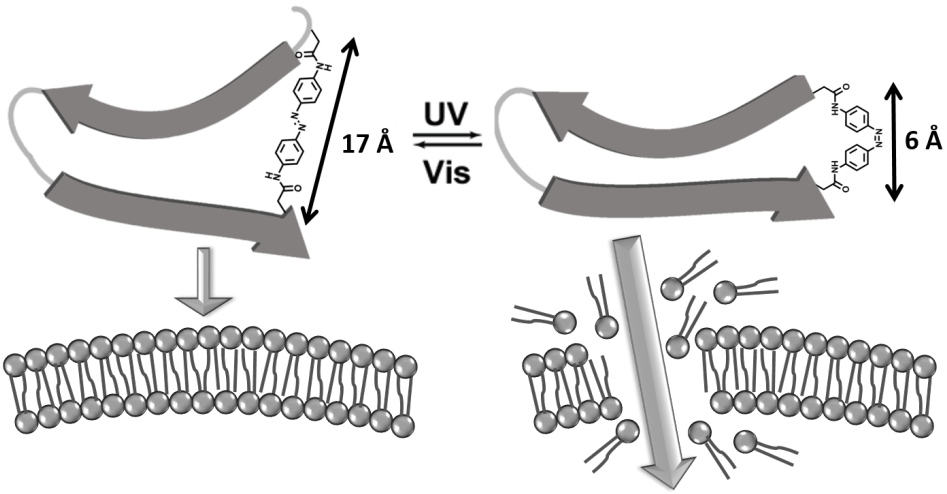

Scheme 3. General scheme of Ab-AR-1 peptide.

Ab-stapling at Cys3 and Cys20 positions of β-sheet AR-1 peptides would be effective for conformational stabilization at the *cis* state because the distance between two Cys residues on AR-1 is about 2.05 Å, which is in accordance with the distance between the *para*-substituents of the *cis* state of the Ab linker.[50] Based on the rationales, Ab-stapled AR-1 peptide (Ab-AR-1) was prepared by the coupling reactions between the Ab compound and the cysteine in the AR-1 peptide (Scheme 3). The AR-1 peptide were purchased from ANYGEN (South Korea). Their molecular weights were confirmed using MALDI-TOF (Figure 20).

4.2 Photo-induced conformational change of the Ab-AR-1 peptide

The photo-induced isomerization of Ab moieties in the Ab-AR-1 peptide was examined by UV/Vis spectrometry (**Figure 22**). Upon 1 min UV irradiation (λ_{max} = 365 nm) on the Ab-AR-1 peptide, the strong $\pi-\pi^*$ absorption band at approximately 360 nm was significantly reduced, whereas the weak $n-\pi^*$ absorption band at approximately 450 nm was slightly increased. The spectral change is a characteristic phenomenon of the *trans-cis* Ab conversion.[51] Conversely, the initial spectrum was supposed to be mostly recovered by Vis irradiation (λ_{max} = 445 nm) for 10 min, indicating that the Ab moiety gets reversibly isomerized even in the Ab-AR-1 peptide structure. However, it recovered into *trans* isomers only 41% of initial spectrum even irradiate 440 nm for more than 10 min. Applied heat 50℃ for 30 min can revert to *trans* isomer (82%) thermodynamically in another method. The change in the helical conformation of the Ab-LK peptide was analyzed by Circular Dichroism (CD) in 50 % PBS/TFE (**Figure 23**). Unexpectedly, the UV irradiated Ab-AR-1 represented rather decrease in β-sheet comparing non-stapled AR-1. As shown in **Figure 23**, compared with the non-stapled AR-1 peptide with a

β-sheet of 74%, the *trans* form of Ab-AR-1 peptide represented insignificantly different β-sheet (63-64%), whereas the UV-induced *cis* form of Ab-AR-1 peptide represented decrease in β-sheet (47-49%). Stapled peptides generally are expected to show higher secondary structure than non-stapled ones because of their lower degree of freedom.[52] The stapling with a too long *trans* Ab linker had a negligible effect on the stabilization of the β-sheet conformation. On the contrary, the *cis* Ab stapling with an appropriate length could significantly stabilize the β-sheet conformation. The choice of the Ab stapling points on the AR-1 peptide was successful in inducing a notable change in the β-sheet conformation. **Figure 23** represents the reversible control of β-sheet by serial UV-Vis irradiation. Slightly higher β-sheet (63-64%) of the Vis-irradiated samples than the initial β-sheet (74%) of 100% *trans* form might be due to the 82% recovery of the *trans* form by heating 50℃ for 30 min (**Figure 24**). In summary, the results indicated that the β-sheet secondary structure of the AR-1 peptide could be effectively and reversibly regulated by mild light signals (8 and 5 mW/cm^2 for UV and Vis, respectively) and heating for a while.

4.3 Photo-switching of antimicrobial activity of the Ab-AR-1 peptide

The bactericidal activities of the Ab-AR-1 peptides against *E. coli* (ATCC 25922), a representative gram-negative bacterium, are shown as minimum inhibitory concentration (MIC). (Figure 24). After 20 h incubation, the AR-1 peptide without Ab stapling showed higher demolishing activity against *E. coli* (MIC = 4 μM), irrespective of the UV irradiation. However, the Ab-AR-1 peptide showed a dramatic change bactericidal activities responding to UV light. Non-irradiated Ab-AR-1 peptide with mostly *trans* forms showed almost lost bactericidal activity against *E. coli*, whereas UV-irradiated Ab-AR-1 peptide mainly in the *cis* form showed 54% bactericidal activity at 32 μM. In a previous report, Feringa's group showed that antibacterial activity of quinolone based antibacterial agent could be controlled by photo-irradiation.[53] They used Azobenze-quinolone through *cis-trans* conversion of an Ab-linker for the bactericidal activity control at micromolar concentrations (≥ 16 μg/mL).

4.4 Preparation of the Photo-caged *o*-Nb-AR-1 peptide

Since the bactericidal activity of the Ab-AR-1 peptide against *E. coli* was not satisfied, two *ortho*-nitrobenzyl groups were applied to on each thiol residues of cysteines of AR-1. The synthetic scheme is shown in Scheme 4.

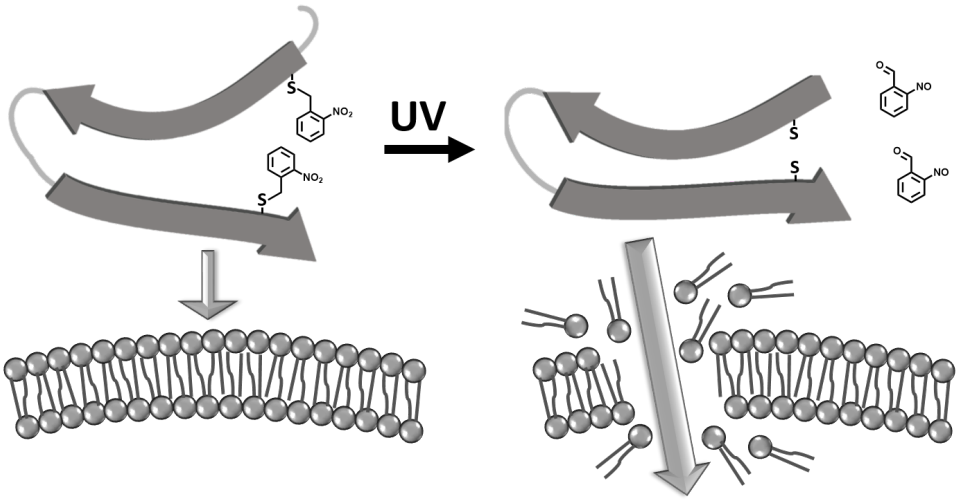

Scheme 4. General scheme of *o*-Nb-AR-1 peptide.

ortho-Nitrobenzyl (*o*-Nb) is a commonly used photolabile group as photo-cage.[54] Covalently linking an *o*-Nb moiety on AR-1 peptide yields *o*-Nb-AR-1 peptide (Figure 25). Excess of *ortho*-Nitrobenzyl bromide was reacted with the AR-1 peptide (sequence: RWCVYAYVRVRGVLVRYRRCW) in the presence of tris(2-carboxyethyl)phosphine hydrochloride (TCEP) to prevent forming disulfide bond during the coupling reaction. The AR-1 peptide (0.5

mM) and tris(2-carboxyethyl)phosphine hydrochloride (TCEP) (1 mM) were dissolved in an aqueous solution containing 100 mM Tris-HCl buffer solution (pH 8.0). The reaction mixture was allowed to be stirred for an hour at ambient temperature. The *ortho*-Nitrobenzyl bromide (2.5 mM) was dissolved in DMF and the solution was mixed with the peptide solution. After 24 h-stirring, the photo-caged peptide (Ab-AR-1) was purified using HPLC with the same protocol described above.

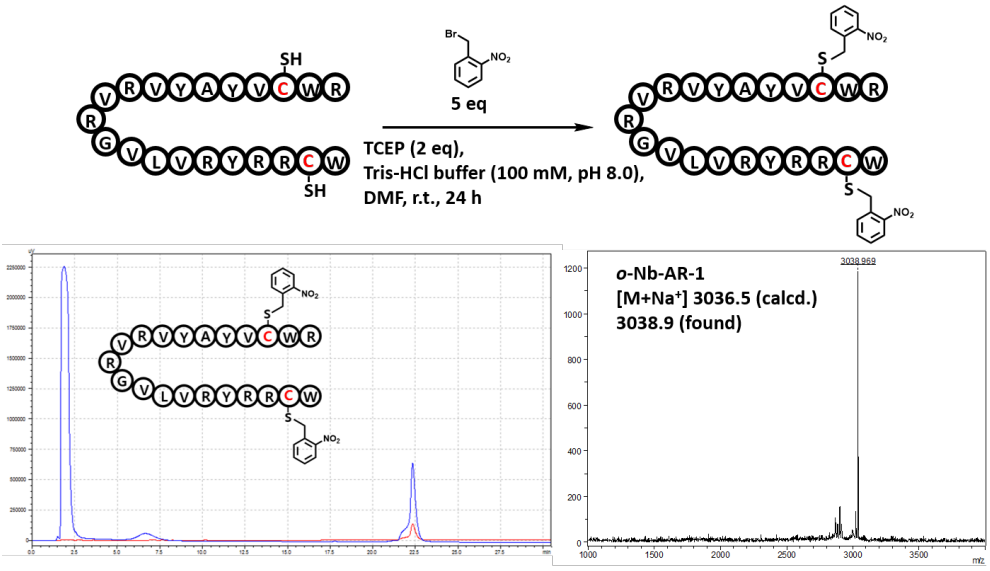

Figure 25. sequence: *o*-Nb-RWCVYAYVRVRGVLVRYRRCW was obtained at 22.4 min as white powder with eluted 20 to 50% of ACN 0.1% TFA for 30 min. The HPLC chromatogram of *o*-Nb-AR-1 is shown (left, bottom) with detection at 220 nm (black) and 280 nm (red). MS ($M+Na^+$) 3036.5 (calcd.), 3038.9 (found) (bottom)

4.5 Photo-induced conformational change of the *o*-Nb-AR-1 peptide

Irradiating a certain wavelength of light to modified *o*-Nb-AR-1 peptide generates the uncaged AR-1 expected to recover the antimicrobial activity by stabilizing of the β-sheet conformation. To minimize the basal antimicrobial activity without irradiation, it is decided to disrupt the β-sheet conformation through blocking two cysteine for disulfide bridge. The photo-caged of *o*-Nb-AR-1 peptide was examined by UV/Vis spectrometry (Figure 26a). Upon 5 min UV irradiation (λ_{max} = 280 nm) on the *o*-Nb-AR-1 peptide, the strong absorption in the range of 250-280 nm was significantly reduced, whereas the weak absorption band at approximately 340 nm was slightly increased. The spectral change is a characteristic phenomenon of existence 2-nitrosobenzaldehyde[55] indicating that the original AR-1 gets returned.

Circular Dichroism (CD) in 50 % PBS/TFE (Figure 26b). The *o*-Nb-AR-1 represented remarkably decrease in β-sheet comparing AR-1. As shown in Figure 23 and 26, compared with the AR-1 peptide with a β-sheet of 74%, the *o*-Nb-AR-1 peptide represented significantly different β-sheet (15%), whereas the

UV-induced de-protection form of *o*-Nb-AR-1 peptide represented recover only 1% in β-sheet (16%). The conjugation with *o*-Nb groups had a dramatic effect on the de-stabilization of the β-sheet conformation. On the contrary, upon UV irradiation induced detachment of *o*-Nb groups were expected to enhance the β-sheet conformation. However, it was not successful in inducing a notable change in the β-sheet conformation. **Figure 26b** represents the control of β-sheet by UV irradiation. In summary, the results indicated that the β-sheet secondary structure of the AR-1 peptide could not be effectively regulated by light signals.

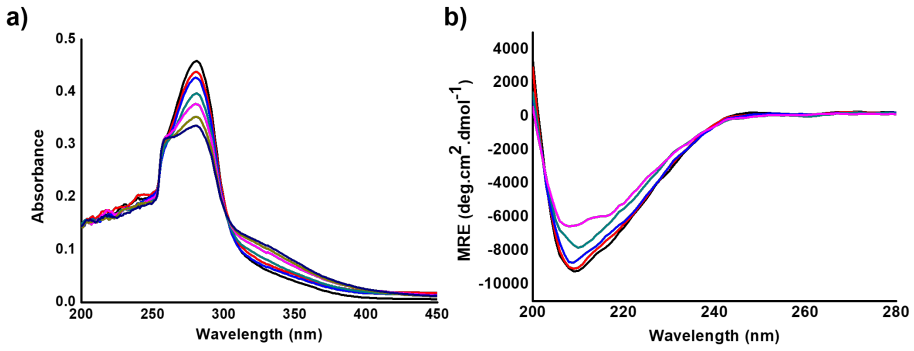

Figure 26. (a) UV/Vis absorption spectral changes of *o*-Nb-AR-1 (25 μM in 50 mM PBS pH 7.4, 25℃) upon irradiation at 280 nm for 5 min. (b) CD spectral changes of Ab-AR-1 (100 μM in 50 mM PBS and 50% TFE) upon irradiation 280 nm for 20 min.

4.6 Photo-cleavage change of the *o*-Nb-AR-1 peptide

The photo-cleavage of *o*-Nb-AR-1 peptide showed significant change on mass spectrum upon UV irradiation (Figure 27). MALDI-TOF mass spectrometry was carried out for the analysis of photo-cleavage of *o*-Nb-AR-1 peptide depending on UV irradiation. A Bruker DE/micro flex LT mass spectrometer equipped with a nitrogen UV laser (337 nm) was used for the analysis. Generally, α-Cyano-4-hydroxy-cinnamic acid (CHCA) was used as the matrix. 640 μM of sample were prepared in DMSO and 2 μL were mixed with another 2 μL of saturated CHCA in (50% DW/ ACN). After measurement, the solution was irradiated UV light, which resulted in photo-cleavage of *o*-Nb groups. Irradiation was carried out using a 100 W high-pressure mercury lamp (Lichtzen, South Korea). For 1 min irradiation, the large difference showing on mass spectrum indicating an effective photo-cleavage. Recover AR-1 from photo-cleavage of *o*-Nb-AR-1 peptide can have a potential to be used as a spatiotemporally controllable antimicrobial activity.

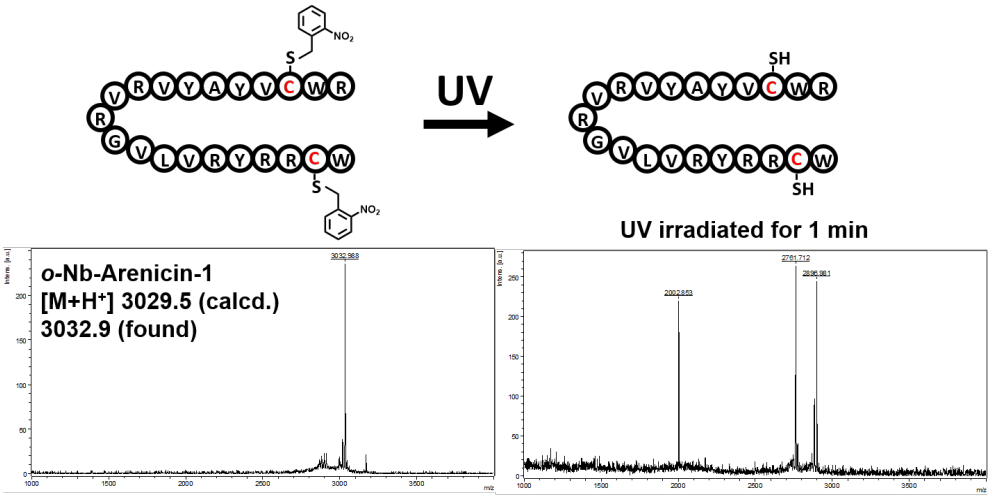

Figure 27. General scheme for photo-cleavage of *o*-Nb-AR-1 peptide and mass spectral changes of *o*-Nb-AR-1 upon irradiation at 280 nm for 1 min. MS ($M+H^+$) 3029.5 (calcd.), 3032.9 (found) (left, bottom). Irradiated *o*-Nb-AR-1 were found as photo-cleaved AR-1 ($M+H^+$) 2759.5 (calcd.), 2761.7 (found) (left, bottom).

4.3 Photo-induced of antimicrobial activity of the *o*-Nb-AR-1 peptide

The bactericidal activities of the *o*-Nb-AR-1 peptides against *E. coli* (ATCC 25922), a representative gram-negative bacterium, are shown as minimum inhibitory concentration (MIC). (Figure 28). Peptides were prepared by 2-fold dilution method in DW/DMSO because of poor solubility in water. Final DMSO volumn percent was kept below 5 % which does not affect a bacteria growth conditions. After 20 h incubation, the AR-1 peptide without Ab stapling showed higher demolishing activity against *E. coli* (MIC = 16 μM), irrespective of the UV irradiation. However, the *o*-Nb-AR-1 peptide showed a dramatic change bactericidal activities responding to UV light. Non-irradiated Ab-AR-1 peptide with mostly *trans* forms showed almost lost bactericidal activity against *E. coli*, whereas UV-irradiated Ab-AR-1 peptide mainly in the *cis* form showed 41% bactericidal activity at 32 μM.

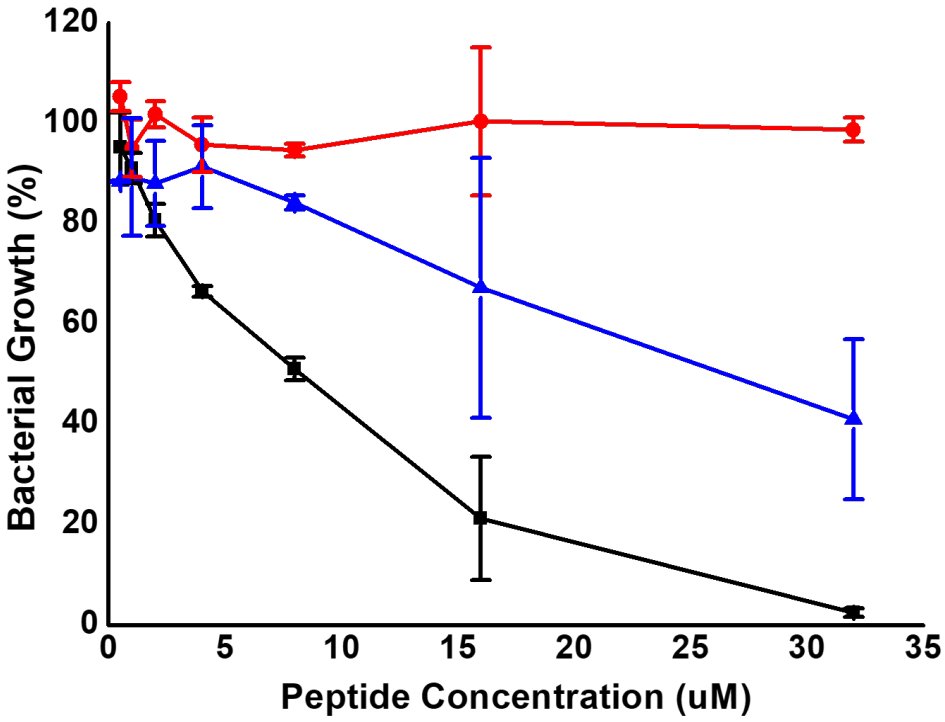

Figure 28. Bacterial growth spectrum depending on concentration of AR-1 (black) and *o*-Nb-AR-1 (0.5 to 32 μM incubated for 20h at 37℃)were measured the absorbance at 600 nm. Non-irradiated *o*-Nb-AR-1 (red) and irradiated *o*-Nb-AR-1 (blue) were shown.

5. Conclusion

In this study, it is demonstrated that antimicrobial of peptides can be controlled by photo-caged *o*-Nb-AR-1. The antimicrobial activity of the *o*-Nb-AR-1 peptide can be effectively regulated by photo-cleavage of *o*-Nb groups. The β-sheet conformation was selectively recovered by UV-cleavage of the photo-caged *o*-Nb-AR-1 peptide, and the regenerated AR-1 showed clear enhancement of antimicrobial activities compared with the non-irradiated *o*-Nb-AR-1 peptide with restoring secondary structure. The remarkable dependence of antimicrobial activity on the secondary structure as well as the light-activation might be important information for future development of highly selective antibiotic agents. Furthermore, photo-caged of antibacterial activity would be an effective drug targeting strategy with outstanding spatiotemporal specificity.

6. Reference.

[32] Ventola, C. L. The Antibiotic Resistance Crisis. *P. T.* 2015, *40*, 277-283.

[33] Coates. A.; Hu. Y.; Bax. R.; Page. C. The Future Challenges Facing the Development of New Antimicrobial Drugs. *Nat. Rev. Drug. Discov*. 2002, *1*, 895-910.

[34] Zasloff. M. Antimicrobial peptides of multicellular organisms. *Nature*. 2002, *415*, 389-395.

[35] Hancock. R. E.; Sahl. H. G. Antimicrobial and host-defense peptides as new anti-infective therapeutic strategies. *Nat Biotechnol*. 2006, *24*, 1551-1557.

[36] Lazzaro. B. P.; Zasloff. M.; Rolff. J. Antimicrobial peptides: Application informed by evolution. *Science*. 2020, *368*, 487-494.

[37] Zasloff. M. Antibiotic peptides as mediators of innate immunity. *Curr. Opin. Immunol*. 1992, *4*, 3-7.

[38] Hancock, R. E. W.; Diamond, G. The role of cationic antimicrobial peptides in innate host defences. *Trends Microbiol*. 2000, *8*, 402-410.

[39] Ovchinnikova, T. V.; Aleshina, G. M.; Balandin, S. V.; Krasnosdembskaya, A. D.; Markelov, M. L.; Flolova, E. I.; Leonova, Y. F.; Tagaev, A. A.; Krasnosdembskay, E. G.; Kokryakov, V. N. *FEBS Lett*. 2004, *577*, 209-214.

[40] Orlov, D. S.; Shamova, O. V.; Eliseev, I .E.; Zharkova, M. S.; Chakchir, O. B.; Antcheva, N.; Zachariev, S.; Panteleev, P. V.; Kokryakov, V. N.; Ovchinnikova, T. V.; Tossi, A. Redesigning Arenicin-1, an Antimicrobial Peptide from the Marine Polychaeta *Arenicola marina*, by Strand Rearrangement or Branching,

Substitution of Specific Residues, and Backbone Linearization or Cyclization. *Mar. Drugs*. 2019, *17*, 376-397.

[41] Szymański, W.; Beierle, J. M.; Kistemaker, H. A. V.; Velema, W. A.; Feringa, B. N. Reversible Photocontrol of Biological Systems by the Incorporation of Molecular Photoswitches. *Chem. Rev.* 2013, *113*, 6114-6178.

[42] Mayer, G.; Heckel, A. Biologically active molecules with a "light switch". *Angew. Chem. Int. Ed. Engl*, 2006, *45*, 4900-4921.

[43] Gorostiza, P.; Isacoff, E. Y. Optical switches for remote and noninvasive control of cell signaling. *Science*, 2008, *322*, 395-399.

[44] Koçer, A.; Walko, M.; Meijberg, W.; Feringa, B. L. A Light-Actuated Nanovalve Derived from a Channel Protein. *Science.* 2005, *309*, 755-758.

[45] (a) Dhammika Bandara, H. M.; Burdette, S. C. Photoisomerization in Different Classes of Azobenzene. *Chem. Soc. Rev.* 2012, *41*, 1809-1821. 1510. (b) Mart, R. J.; Allemann, R. K. Azobenzene Photocontrol of Peptides and Proteins. *Chem. Commun.* 2016, *52*, 12262-12277.

[46] (a) Kim, Y.; Philips, J. A.; Liu, H.; Kang, H.; Tan, W. Using Photons to Manipulate Enzyme Inhibition by an Azobenzene-Modified Nucleic Acid Probe. *Proc. Natl. Acad. Sci. U. S. A.* 2009, *106*, 6489-6494. (b) Schierling, B.; Noël, A-J.; Wende,W.; Hien, L .T.; Volkov, E.; Kubareva, E.; Oretskaya, T.; Kokkinidis, M.; Römpp, A.; Spengler, B.; Pingoud, A. Controlling The Enzymatic Activity of a Restriction Enzyme by Light. *Proc. Natl. Acad. Sci. U. S. A.* 2010, *107*, 1361-1366.

[47] (a) Schrader, T. E.; Schreier, W. J.; Cordes, T.; Koller, F. O.; Babitzki, G.; Denschlag, R.; Renner, C.; Löweneck, M.; Dong, S-

L.; Moroder, L.; Tavan, P.; Zinth, W. Light-triggered β-hairpin folding and unfolding. *Proc. Natl. Acad. Sci. U. S. A.* 2007, *104*, 15729-15734. (b) Aemissegger, A.; Kräutler, V.; van Gunsteren, W. F.; Hilvert, D. A Photoinducible β-Hairpin. J. Am. Chem. Soc. 2005, *127*, 2929-2936.

[48] Liu, G.; Dong, C-M. Photoresponsive Poly(S-(o-nitrobenzyl)-l-cysteine)-b-PEO from a l-Cysteine N-Carboxyanhydride Monomer: Synthesis, Self-Assembly, and Phototriggered Drug Release. *Biomacromolecules.* 2012, *13*, 1573-1583.

[49] Shamay, Y.; Adar, L.; Ashkenasy, G.; David, A. Light induced drug delivery into cancer cells. *Biomaterials*. 2011, *32*, 1377-1386.

[50] Bellotto, S.; Chen, S.; Rebollo, I. R.; Wegner, H. A.; Heinis, C. Phage Selection of Photoswitchable Peptide Ligands. *J. Am. Chem. Soc.* 2014, *136*, 5880-5883.

[51] (a) Samanta, S.; Woolley, G. A. Bis-Azobenzen Crosslinkers for Photocontrol of Peptide Structure. *ChemBioChem* 2011, *12*, 1712-1723. (b) Hamm, P.; Ohline, S. M.; Zinth, W. Vibrational Cooling After Ultrafast Photoisomerization of Azobenzene Measured by Femtosecond Infrared Spectroscopy. *J. Chem. Phys.* 1997, *106*, 519-529..

[52] Grison, C. M.; Burslem, G. M.; Miles, J. A.; Pilsl, L. K. A.; Yeo, D. J.; Imani, Z.; Warriner, S. L.; Webb, M. E.; Wilson, A. J. Double Quick, Double Click Reversible Peptide "Stapling". *Chem. Sci.* 2017, *8*, 5166-5171.

[53] Velema, W. A.; van der Berg. J. P,; Hansen. M. J.; Szymanski. W.; Driessen. A. J. M.; Feringa. B. L. Optical Control of Antibacterial Activity. *Nat. Chem.* 2013, *5*, 924-928.

[54] Klán, P.; Šolomek, T.; Bochet, C. G.; Blanc, A.; Givens, R.; Rubina, M.; Popik, V.; Kostikov, A.; Wirz, J. Photoremovable Protecting Groups in Chemistry and Biology: Reaction Mechanisms and Efficacy. *Chem. Rev.* 2013, *113*, 119-191.

[55] Il'ichev, Y. V.; Schwörer, M. A.; Wirz, J. Photochemical Reaction Mechanisms of 2-Nitrobenzyl Compounds: Methyl Ethers and Caged ATP. *J. Am. Chem. Soc.* 2004, *126*, 4581-4595.

Abstract in Korean (국문 초록)

펩타이드는 일반적으로 50 개 이하의 아미노산이 아마이드 결합 또는 펩타이드 결합으로 연결되어, 아미노 수소 원자와 카복실 산소 원자 사이의 수소 결합 패턴에 의해 이차 구조를 가진다. 대표적인 이차 구조로는 알파 나선 (α-helix) 구조와 베타 병풍 (β-sheet) 구조가 있으며, 이의 생화학적 기능으로 단백질의 3 차 구조를 구성하는 요소로 조효소 및 보조 인자와 같은 리간드 또는 DNA, RNA 와 같은 거대분자와의 결합에 관여한다. 따라서, 펩타이드의 이차 구조 변화를 유도하였을 경우, 그에 따른 생화학적 기능의 변화 또한 기대할 수 있다.

빛이란 외부 자극 중, 가장 빠르고 자극이 적으며, 특히 마이크로미터 이하 수준의 미세한 조절도 가능하기에 외부 자극으로 특히 주목을 받고 있다. 따라서 빛 감응성 물질은 빛으로 원하는 시간과 장소에서만 선택적으로 화학적 결합을 끊어내거나 화학 분자의 이성질화를 유도 할 수 있어 펩타이드의 이차 구조를 변화시켜 생화학적 기능을 바꿀 수 있는 매우 효과적인 전략이다.

본 박사학위 논문은 1) 빛에 의하여 트랜스- 와 시스- 두 가지 구조 이성질체를 가지는 아조벤젠 (azobenzene)을 기반으로 분자의 길이가 다른 이성질체의 구조적인 특성을 이용하여 알파 나선 이차 구조의 변화를 유도하며 선택적인 세포 투과성을 가지는 LK 펩타이드 사례와 2) 빛에 의하여 화학적 결합이 끊어지는 오쏘-나이트로벤질 (*o*-nitrobenzyl) 분자를 활용하여 항균성 펩타이드가 가지는 베타 병풍 구조의 변화를 유도하여 선택적인 항균성 AR-1 펩타이드 사례를 보고한다. 이는 펩타이드의 대표적인 두 가지 이차 구조인 알파 나선 구조와 베타 병풍 구조를 각각 빛에 의한 구조 변화를 유도하고 그에 따른 생화학적 기능 변화를 보고한다.

첫번째로 다양한 세포 투과성 펩타이드 중, LK 펩타이드는 양극을 띄는 라이신 (Lys, K)과 소수성의 루신 (Leu, L)이 잘 정렬된 구조를 기반으로 양쪽성 구역이 잘 구별된 알파 나선 구조를 가진다. 이를 기반으로 매우 효율적인 세포 투과성을 나노 몰 농도 수준에서도 나타내지만, 무분별한 세포 투과로 인한 부작용을 억제하는 방법 또한 매우 중요하다. 따라서, LK 펩타이드의 선택적인 세포 투과성을 위하여, 광이성질체화 특성을 갖는 아조벤젠을 LK 펩타이드에 도입하였다. 아조벤젠은 N=N 결합을 중심으로 양쪽에 두개의 페닐 그룹을 포함하고 있으며, 빛에 의한 트랜스-, 시스- 형태로 가역적인 변화가 가능하다. 아조벤젠이 연결된 LK 펩타이드는 아조벤젠의 구조 변화로 인하여 알파 나선 구조가 재배열 되며, 그에 따른 세포 투과성 차이도 유발하였다. 트랜스 형태의 아조벤젠은 LK 펩타이드를 펼치면서 알파 나선 구조를 망가트리고 세포 투과성도 감소시킨 반면, UV 빛을 받아 변화한 시스 형태의 아조벤젠은 LK 펩타이드의 알파 나선 구조를 강화하면서 훨씬 향상 된 세포 투과성을 나타냈다.

두번째로 항균성 펩타이드인 AR-1 펩타이드는 바다지렁이 (*Arenicola marina*)에서 추출된 물질로, 양전하를 띄는 6 개의 아르기닌 (Arg, R)을 포함하고 있으며, 두개의 시스테인 (Cys, C) 사이의 이황화 결합 (Cys3-Cys20)을 가진다. 이는 베타 병풍 구조를 형성하며, 박테리아의 세포막을 망가트리는 기작을 통하여 세균을 죽이는 것으로 알려져 있다. 하지만 이러한 기작은 원핵세포인 병원균뿐만이 아닌 진핵세포에도 비슷한 영향을 주어 적혈구 세포의 용혈 현상을 유발하는 부작용을 보인다. 따라서, 선택적으로 원핵세포인 병원균에서만 기작을 유발하기 위하여 AR-1 펩타이드에 빛 감응성 분자인 오쏘-나이트릴 벤질 그룹을 도입하였다. 2 개의 오쏘-나이트로 벤질 그룹을 AR-1 펩타이드의 시스테인 각각에 결합하여 이황화 결합 형성을 방해하는 동시에 베타 병풍 구조 형성을 제한하여 항생 효과를 억제하였다.

하지만, UV 빛을 쪼여주어 보호 그룹이 떨어진 이후, AR-1 펩타이드는 원래의 베타 병풍 구조와 항균성을 회복하였다.

본 논문은 펩타이드의 이차 구조 변화를 유도하여 선택적 세포 투과성 및 항균성 조절에 대한 생화학적 활성을 제어하는 방법을 제시하였다. 빛이라는 외부 자극을 통하여 빛에 감응하는 아조벤젠 분자의 구조적 변화를 통한 알파 나선형 구조의 세포 투과성 펩타이드와 오쏘-나이트로벤질 그룹의 선택적 화학결합을 끊어내는 방법을 통한 베타 병풍 구조의 항균성 펩타이드의 이차 구조 변화를 유도하여 그에 따른 활성을 변화시킬 수 있다는 것을 증명하였다. 더 나아가서는 부작용을 줄일 수 있는 선택적이고 보다 안전한 세포내 전달과 항균성을 조절할 수 있는 전략으로서의 발전 가능성을 제시하였다.

주요어: 알파 나선 구조, 세포 투과성 펩타이드, 아조벤젠, 베타 병풍 구조, 항균성 펩타이드, 오쏘-나이트로 벤질

학번: 2015-30097